

# Gondwana break-up related magmatism in the Falkland Islands

M. J. Hole<sup>1</sup>, R.M. Ellam<sup>2</sup>, D.I.M. MacDonald<sup>1</sup> & S.P. Kelley<sup>3</sup>

<sup>1</sup>*Department of Geology & Petroleum Geology University of Aberdeen, AB24 3UE, UK*

<sup>2</sup>*Scottish Universities Environment Research Centre, East Kilbride, Glasgow, G75 0QU, UK*

<sup>3</sup>*Department of Earth & Environmental Sciences, Open University, Milton Keynes, MK7 6AA UK*

Jurassic dykes (c. 182 Ma) are widespread across the Falkland Islands and exhibit considerable geochemical variability. Orthopyroxene-bearing NW-SE oriented quartz-tholeiite dykes underwent fractional crystallization > 1 GPa, and major element constraints suggest that they were derived by melting of pyroxenite-rich source. They have  $\epsilon\text{Nd}_{182}$  in the range -6 to -11 and  $^{87}\text{Sr}/^{86}\text{Sr}_{182} > 0.710$  and therefore require an old lithospheric component in their source. A suite of basaltic-andesites and andesites exhibit geochemical compositions transitional between Ferrar and Karoo magma types, and are similar to those seen in the KwaZulu-Natal region of southern Africa and the Theron Mountains of Antarctica. Olivine-phyric intrusions equilibrated at < 0.5 GPa, and have isotopic compositions ( $\epsilon\text{Nd}_{182}$  1.6-3.6 and  $^{87}\text{Sr}/^{86}\text{Sr}_{182}$  0.7036-0.7058) that require limited interaction with old continental lithosphere. A suite of plagioclase-phyric intrusions with  $^{87}\text{Sr}/^{86}\text{Sr}_{182}$  c. 0.7035 and  $\epsilon\text{Nd}_{182}$  c. +4, and low Th/Ta and La/Ta ratios (c. 1 and c. 15 respectively) also largely escaped interaction with the lithosphere. These isotopically depleted intrusions were probably emplaced synchronously with Gondwana fragmentation and the formation of new oceanic lithosphere. Estimates of mantle potential temperature from olivine equilibration temperatures do not provide unequivocal evidence for the presence of a plume thermal anomaly beneath the Falkland Islands at 182 Ma.

25 The Early Jurassic (c. 180 Ma) Karoo and Ferrar large igneous provinces (LIP) were associated  
26 with Gondwana break-up. Igneous rocks of the Karoo province occur predominantly in South  
27 Africa but extend into Dronning Maud Land (Antarctica) with the main phase of activity taking  
28 place in the interval 182-183 Ma (Svensen *et al.* 2012). The Ferrar Province, which is  
29 contemporaneous with the magmatism in the Karoo province (Burgess *et al.* 2015), is typified  
30 by the low TiO<sub>2</sub> Jurassic igneous rocks of the Transantarctic Mountains and Tasmania (Hergt *et*  
31 *al.* 1989; Fleming *et al.* 1995). It has also been established that the Karoo and Ferrar provinces  
32 have areas of geographical overlap, most notably in the KwaZulu area of South Africa (Sweeney  
33 *et al.* 1994; Riley *et al.* 2006) and in the Theron Mountains of Antarctica (Brewer *et al.* 1992).  
34 In the latter, at least four suites of low TiO<sub>2</sub> igneous rocks have been recognized, and it has been  
35 suggested that there is a transition from one province to the other rather, than a strict  
36 geographical delineation between the two provinces (Brewer *et al.* 1992).

37 Elliott & Fleming (2000) argued that the principal focus of magmatism for both the Karoo  
38 and Ferrar provinces was the Weddell Triple Junction (Fig. 1) which was within the envelope of  
39 a plume-related thermal anomaly associated with Gondwana break-up. Prior to Gondwana  
40 fragmentation, plate reconstructions place the Falkland Islands on the extension of the Cape  
41 Fold Belt of South Africa, on the eastern flank of the Lebombo Rift (Fig. 1; Macdonald *et al.*  
42 2003; Stone *et al.* 2008; 2009; Richards *et al.* 2013). Post-180 Ma, there was major re-  
43 organization of crustal blocks in Patagonia, the Falklands Plateau and west Antarctica, which  
44 included the clockwise rotation of the Falklands crustal block in an overall extensional regime.  
45 The 180° rotation of the Falkland Islands from their pre-180 Ma position was complete by 165  
46 Ma (Macdonald *et al.* 2003), and by this time the islands had migrated to the west along the  
47 extension of the Aghulas Fracture zone to a position well to the west of the WTJ (Richards *et al.*  
48 2013). Consequently, the Falkland Islands may have been very close to the focus of break-up  
49 related magmatism, and it is logical to assume that the geochemical composition of any igneous  
50 rocks found in the islands should reflect the diversity of magmatism in the Jurassic Gondwana

LIP as a whole. In this paper, new data are presented that show that the dykes and minor intrusions of the Falkland Islands exhibit variability in mineralogy, major element, trace element and Sr-, Nd- and Pb-isotopic compositions that is nearly as large as that seen in the entire Jurassic Gondwana LIP, even though the Falkland Islands themselves represent only an extremely small area compared to the total distribution of Jurassic igneous rocks of the region. Intrusions with major and trace element characteristics most similar the Ferrar dolerites of the Transantarctic Mountain are juxtaposed with intrusions which are nearly identical to some Karoo basalts of South Africa and Antarctica.

### **Falkland Islands Dyke Swarm**

Dolerite dykes, mostly of Jurassic age, are widespread in West Falkland and rather sparse in East Falkland (Fig. 2; Greenway 1972; Mussett & Taylor 1994; Thistlewood *et al.* 1997; Mitchell *et al.* 1999; Stone *et al.* 2008, 2009; Richards *et al.* 2013). Distinct sub-swarms of dykes have been recognized based on azimuth of exposed intrusions and aeromagnetic anomalies (Mitchell *et al.* 1999; Stone *et al.* 2009). Prominent dolerite dykes, tens of metres wide and oriented NE-SW, are present in both West and East Falkland and are reversely magnetized. This suite corresponds to the N-S suite of Mitchell *et al.* (1999), and is of Jurassic age (c. 178-190 Ma; Mussett & Taylor 1994; Stone *et al.* 2009) although the older of these ages were generated by the Ar-Ar method on whole-rock samples and have large errors (e.g R1790 190±4 Ma; Mussett & Taylor 1994). E-W oriented olivine-dolerite dykes occur locally in the south of West Falkland, and they form part of a larger suite of intrusions that Stone *et al.* (2009) suggest has a partially radial disposition. In addition, Richards *et al.* (2013) noted that there is a suite of about 40, N-S oriented magnetic anomalies, that may represent intrusions, and these occur across the entire Falkland Islands. Exposed examples from Teal Creek and Peat Banks (Fig. 2) yield  $^{40}\text{Ar}/^{39}\text{Ar}$  ages in the range 133-138 Ma and these dykes are likely to be members of the Etendeka suite of south-western Africa (Stone *et al.* 2009; Richards *et al.* 2013). During the current study,  $^{40}\text{Ar}/^{39}\text{Ar}$  step-heating analysis was carried-out on separated plagioclase

feldspar phenocrysts from three samples, but only one of these yielded useful information. Sample WI-5, a NE-SW oriented dyke from Weddell Island (Fig. 2), which is also within the area of the radial swarm identified by Richards *et al.* (2013), contains abundant plagioclase phenocrysts, and yielded a precise age of  $182.3 \pm 1.5$  Ma (Fig. 3). This confirms a Jurassic age for some of the Falkland Islands intrusions, and it is within error of the  $178.6 \pm 4.9$  Ma determined by Stone *et al.* (2008) for an aphyric NE-SW dyke from Port Sussex Creek, East Falkland (Fig. 2).

Selected major and trace element abundances *versus* weight % MgO for 139 intrusions from the Falkland Islands, including 109 from this study and 30 from Mitchell *et al.* (1999), are shown in Fig. 4 and representative analyses are given in Table 1. Mitchell *et al.* (1999) divided the intrusions of the Falkland Islands into two main N-S and E-W suites based on azimuth, field occurrence, petrography, mineral chemistry and whole-rock geochemical data. A subsidiary three magma types were also tentatively identified by Mitchell *et al.* (1999), including ‘evolved N-S’, Lively Island and Mount Alice types. The reassessment of the spatial distribution, orientation and age of the dyke swarms by Stone *et al.* (2009) and Richards *et al.* (2013), along with the much enlarged data set for the igneous rocks of the Falkland Islands generated for this study, now allows the identification of five individual geochemical types of intrusions. The criteria used to separate the different groups of intrusions are given in Table 2 and are illustrated in Figs 4 to 9. A description of each suite is given below.

**Port Sussex Creek-type intrusions (PST).** All the N-S dykes of Mitchell *et al.* (1999) are included in this suite of intrusions, with the exception of the ‘evolved type’ described by Mitchell *et al.* (1999) which will be discussed under the Dyke Island Type (samples NHF17 and NGF15). PST intrusions are widely distributed across both East Falkland and West Falkland, all are sub-vertical with an azimuth of NE-SW, and they are consistently between 8 and 10 m in thickness. A typical example occurs at Port Sussex Creek, East Falkland, (MHF1; Table 1, Fig. 2), and is an 8m wide, sub-vertical, medium-grained, spheroidally-weathering dolerite dyke with

an azimuth of 45° (NE-SW) and an age of 178.6±4.9 Ma (Stone *et al.* 2008). The texture is equigranular and intersertal. Pyroxene is enstatite (En<sub>70</sub>Wo<sub>4</sub>Fs<sub>26</sub>), pigeonite (En<sub>51</sub>Wo<sub>13</sub>Fs<sub>36</sub>) and augite (Fig. 5) and the feldspar is labradorite (An<sub>70</sub>). All PST intrusions contain both augite and pigeonite, with more mafic samples containing orthopyroxene. Olivine (Fo<sub>50-71</sub>) is rare in this suite of rocks and is restricted to intrusions with Mg# >58 (e.g. FAR1503 and NGF16; Table 1, Fig. 4). Whole-rock MgO contents vary from 5.9-9.5 wt% (Mg# 50-62) and SiO<sub>2</sub> (53-55wt%) is higher for a given MgO concentration than any of the other Falkland Islands intrusions (Fig. 4). The PST intrusions are characterized by low CaO (8.1-9.8wt%) for a given MgO content compared to other Falkland Islands intrusions. TiO<sub>2</sub> abundances (0.9-1.2wt%) are typical of the low TiO<sub>2</sub> Gondwana break-up related LIPs of the southern hemisphere and distinguishes them from the high TiO<sub>2</sub> (>2.5wt%) suite of break-up related magmas (e.g. Brewer *et al.* 1992). Abundances of Cr are unusually high (up to 648ppm) for samples with SiO<sub>2</sub> in their range, and are reflected in the high Cr content of orthopyroxene. Abundances of Nb and Y are restricted to 2-5 and 19-23ppm respectively. PST intrusions are LREE enriched (Fig. 6) with [La/Yb]<sub>N</sub> in the range 3.2-3.9 and samples lack any significant Eu anomaly (Eu/Eu\* 0.89-0.97). La/Ta and Th/Ta are the highest of any of the Falkland Islands samples analysed (44-52 and 5.9-8.6 respectively), and consequently, on ORB-normalized multi-element diagrams (Fig. 7), samples exhibit a marked trough in the abundances of Ta and Nb relative to Th, U, K and La. [Ta/Yb]<sub>N</sub> is in the range 2.0 to 2.6, the lowest values for any of the Falkland Islands intrusions. Ti/Zr and P/Zr (55-60 and 4.5-6.3 respectively) are such that all PST intrusions exhibit a minor trough at Ti and P relative to adjacent elements on ORB-normalized diagrams. εNd<sub>182</sub> varies from -5.5 to -11.0 and is accompanied by radiogenic Sr-isotopic compositions (<sup>87</sup>Sr/<sup>86</sup>Sr<sub>182</sub> 0.7070-0.7134), although Sr-Nd isotope covariations are rather scattered (Fig. 8). Pb-isotopic compositions form an array that is close to the Geochron (<sup>207</sup>Pb/<sup>204</sup>Pb =15.55-15.65), and extends to <sup>206</sup>Pb/<sup>204</sup>Pb ratios of up to 18.40. <sup>207</sup>Pb/<sup>204</sup>Pb exhibits a negative correlation with εNd<sub>182</sub> for PST intrusions (Fig. 8). Marked negative correlations between 1/Sr and <sup>87</sup>Sr/<sup>86</sup>Sr<sub>182</sub>, εNd<sub>182</sub> and Th/Ta and a

positive correlation between MgO and  $\epsilon\text{Nd}_{182}$  (Fig. 9) suggests that PST dykes underwent interaction with a high  $^{87}\text{Sr}/^{86}\text{Sr}_{182}$  ( $> 0.714$ ), low  $\epsilon\text{Nd}_{182}$  ( $< -12$ ) component that had  $\text{Th}/\text{Ta} > 9$ , and that interaction was concomitant with crystallization

**E-W intrusions.** The E-W samples reported by Mitchell *et al.* (1999) are from a single intrusion, approximately 10m wide, which can be traced for more than 30 km from Fox Bay West to Queen Charlotte Bay (Fig. 2). These samples are generally medium-grained olivine-phyric dolerites ( $\text{Fo}_{82}$  at 11wt% MgO in the whole-rock), the only pyroxene present being augite (Fig. 5). During the current study, intrusions with similar petrographic and mineralogical characteristics were found around South Harbour and on Weddell Island (Fig. 2). E-W intrusions are distinguished from the PST (Fig. 10) by their lower  $\text{SiO}_2$  contents (48-52wt%) and higher  $\text{Ti}/\text{Zr}$  (80-95) for a similar range in  $\text{TiO}_2$ , and MgO content (1.0-1.4 and 4.8-11.4wt % respectively). E-W intrusions have  $[\text{La}/\text{Yb}]_{\text{N}}$  in the range 2.1-4.0 (Fig. 6) and no appreciable Eu anomaly ( $\text{Eu}/\text{Eu}^* = 0.89\text{-}1.0$ ).  $[\text{Ta}/\text{Yb}]_{\text{N}}$  ratios are in the range 2.8 to 4.7, and all samples exhibit a negative Nb, Ta trough relative to the LILE ( $\text{La}/\text{Ta}$ , 16-27,  $\text{Th}/\text{Ta}$  2.2-2.8) but this is not as pronounced as that for the PST intrusions (Fig. 7). E-W intrusions have isotopic compositions that are close to, or slightly depleted relative to the Chondritic Uniform Reservoir ( $\epsilon\text{Nd}_{182} = -0.4$  to  $3.0$ ;  $^{87}\text{Sr}/^{86}\text{Sr}_{182} = 0.7036\text{-}0.7058$ ) and have Pb-isotopic compositions that lie just above the NHRL (Fig. 8).

**Lively Island intrusion.** A single 30m thick intrusion which is exposed on Lively Island has noticeably lower  $\text{TiO}_2$  for a given MgO content than any other of the Falklands Islands intrusions ( $\text{TiO}_2 = 0.8\text{wt}\%$  at  $6\text{wt}\%$  MgO) and the data falls close to the compositional trend for low  $\text{TiO}_2$  Ferrar dolerites from the Transantarctic Mountains (Fig. 11). Characteristic mineralogical features are the presence of sparse, Mg-rich biotite and rare Ca-poor groundmass pyroxene (Fig. 5). The intrusion has a LREE-enriched REE profile ( $[\text{La}/\text{Yb}]_{\text{N}} = 3.2$ ; Fig. 6) which lacks a significant negative Eu anomaly ( $\text{Eu}/\text{Eu}^* = 0.87$ ).  $\text{La}/\text{Ta}$  and  $\text{Th}/\text{Ta}$  (20.4 and 3.2 respectively) are similar to E-W intrusions and considerably lower than for PST intrusions

(Table 2). The Lively Island intrusion contains radiogenic Nd and unradiogenic Sr ( $\epsilon\text{Nd}_{182} -0.5$ ,  $^{87}\text{Sr}/^{86}\text{Sr}_{182}$  c. 0.7060) compared to PST intrusions.

**Dyke Island Type (DIT).** The greatest concentration of DIT intrusions is on aptly-named Dyke Island (Fig. 2). Sample WI-5 which yielded the Ar-Ar age of  $182.3 \pm 1.5$  Ma which crops out on Weddell Island (Fig. 2) is of this type. In addition, the evolved N-S samples described by Mitchell *et al.* (1999) are of this type (e.g. NHF17; Fig. 2). Intrusions are generally <50 cm thick, they may contain abundant plagioclase  $\pm$  augite phenocrysts (samples WI-5, MHF14.9 and FAR338; Fig. 5), or more commonly they are medium- to fine-grained aphyric basaltic-andesites and andesites with rare rhyolite sheets occurring locally. DIT intrusions represent an expanded fractionation series with MgO varying from 5.6 to <0.1wt%, over a range of 51-75wt%  $\text{SiO}_2$ . Ti/Zr is in the range 32-55 for samples with 4.0-5.6wt% MgO, and for samples with <1wt% MgO, Ti/Zr falls to <5 (Fig. 4). All DIT intrusions have higher concentrations of the incompatible elements Zr, Nb and Y than any of the other intrusions from the Falkland Islands, and exhibit strong positive linear correlations between these elements. On a plot of  $\text{TiO}_2$  versus MgO (Figs 4 & 11) DIT intrusions can be divided into three distinct series; i) a low  $\text{TiO}_2$  series which forms an extension of the data array for PST intrusions; ii) a high  $\text{TiO}_2$  series with MgO in the range 2.5-4.0wt% MgO with  $\text{TiO}_2 > 1.7\text{wt}\%$ ; and iii) acid intrusions with <2wt% MgO.

DIT intrusions are LREE-enriched ( $[\text{La}/\text{Yb}]_N = 4.1-6.6$ ; Fig. 6) and exhibit stepwise increases in both LREE and HREE abundances with decreasing MgO with the most evolved sample (MHF41.3, 0.06wt% MgO) having  $\text{La}_N = 190$  and  $\text{Yb}_N = 44$ . The development of a progressively larger negative Eu anomaly ( $\text{Eu}/\text{Eu}^* = 0.85-0.71$ ) with decreasing MgO, attests to the importance of plagioclase fractionation during their petrogenesis. Th/Ta and La/Ta for the DIT intrusions (2.4-3.4 and 17-26 respectively) are similar to those for the E-W intrusions. Multi-element diagrams (Fig. 7) show that DIT intrusions exhibit troughs at Ti and P relative to adjacent elements, and a progressively larger negative Sr anomaly is developed with decreasing



MgO. Plagioclase-phyric samples WI-5 and FAR338 exhibit a positive Sr spike in Fig. 7, which is presumably a result of accumulation of plagioclase feldspar, although neither sample exhibits a Eu anomaly. The distribution of trace elements in DIT intrusions bears a strong resemblance to those for Ferrar dolerites from the Transantarctic Mountains (Fig. 7). DIT intrusions have  $^{87}\text{Sr}/^{86}\text{Sr}_{182}$  in the range 0.7055-0.7170 but all samples with  $^{87}\text{Sr}/^{86}\text{Sr}_{182} > 0.7090$  contain < 2 weight % MgO.  $\epsilon\text{Nd}_{182}$  falls in the range -2.8 to +0.6, and there is no systematic variation between MgO,  $\epsilon\text{Nd}_{182}$  or  $^{87}\text{Sr}/^{86}\text{Sr}_{182}$  (Figs 8 & 9).

**Mount Alice Type intrusions (MAT).** MAT intrusions are restricted to the south-western area of West Falkland, around South Harbour, Dyke Island and Cape Orford (Fig.1) and are early Jurassic in age ( $188 \pm 2$  Ma for sample MA3; Mussett & Taylor 1994). MAT intrusions are generally <1 m thick and are characterized by plagioclase  $\pm$  augite  $\pm$  olivine phenocrysts in a fine-grained groundmass. Since the area in which the MAT intrusions occur is within the region of the radial dyke swarm described Richards *et al.* (2013), azimuths cannot be used as one of their classification criteria, although in the region of Cape Orford, MAT dykes are generally oriented E-W (Mussett & Taylor 1994; Thistlewood *et al.* 1997). A typical example (MFH15.2) contains sparse, scattered phenocrysts of olivine ( $\text{Fo}_{80}$ ), calcic augite ( $\text{En}_{31}\text{Fs}_{25}\text{Wo}_{44}$ ; Fig. 5) and labradorite ( $\text{An}_{60}$ ). MgO varies from 6-12wt%, and the MAT intrusions have the lowest  $\text{SiO}_2$  (46-50wt%) for a given MgO content of any of the Falklands Islands samples (Fig. 4).  $\text{TiO}_2$  abundances (1.3-2.0wt%) overlap with those for both the PST and E-W intrusions but Ti/Zr is in the range 90-150 (Fig. 10) which is considerably higher than any other of the Falkland Islands intrusions. MAT intrusions have  $[\text{La}/\text{Yb}]_{\text{N}}$  in the range 1.8-3.1 (Fig. 6) and flat to slightly LREE-depleted REE profiles for elements La to Sm ( $[\text{La}/\text{Sm}]_{\text{N}}$  0.9-1.5). On multi-element diagrams (Fig. 7), MAT intrusions exhibit a positive Sr spike relative to N-ORB, but otherwise have smooth profiles from elements Nd to Lu, with Ti/Zr and P/Zr (98-130 and 8.0-10.4 respectively) in the range for normal ORB (Ti/Zr c. 100, P/Zr c. 6.9; Sun & McDonough 1987). Unlike all the other Falkland Islands intrusions, the MAT have Th/Ta and La/Ta (0.7-1.0 and



13-17 respectively) which are also within the range for normal ocean ridge basalts and asthenosphere-derived basalts (Sun & McDonough 1987). Sr- & Nd-isotopic compositions fall in the upper-left quadrant of Fig. 8, with  $\epsilon\text{Nd}_{182} > 5$  and  $^{87}\text{Sr}/^{86}\text{Sr}_{182} < 0.7040$ . Pb-isotopic compositions fall just above the NHRL with  $^{206}\text{Pb}/^{204}\text{Pb}$  in the range 18.2-18.5 (Fig. 8).

## **Petrogenesis of the Falkland Islands intrusions**

The diversity of major and trace element geochemistry and isotopic compositions of the Falkland Islands intrusions requires an equally diverse range of petrogenetic histories. In particular, the observed ranges of isotopic compositions described above are likely to require variable interaction between isotopically depleted melts from mantle peridotite with melts derived from continental lithosphere, which in some cases, must of considerable antiquity. Consequently, before attempting to make regional comparisons between the Falkland Islands intrusions and other Gondwana break-up related low  $\text{TiO}_2$  suites within the southern hemisphere, an assessment of the petrogenetic history of each of the suites of Falkland Island intrusions will be made in turn below.

### ***PST intrusions***

PST and low  $\text{TiO}_2$  DIT intrusions exhibit variations in major element compositions that fall along the same fractionation trend as low  $\text{TiO}_2$  basaltic-andesites and andesites from the Theron Mountains (Fig. 11). However, PST and DIT intrusions cannot be related to one another by simple crystal fractionation because their Sr-, Nd- and Pb-isotopic compositions differ significantly from one another (Fig. 8). The high  $^{87}\text{Sr}/^{86}\text{Sr}_{182}$  ( $> 0.710$ ) and unradiogenic Nd-isotopic compositions of the PST is a feature they share with Ferrar Province igneous rocks. Fleming *et al.* (1995) and Molzhan *et al.* (1999) demonstrated that elevated  $^{87}\text{Sr}/^{86}\text{Sr}_{182}$  (0.7090-0.7112) of MFCT basalts was partly a function of Rb and Sr mobility during a Cretaceous (97-125 Ma) hydrothermal event. However, the observed range in  $\epsilon\text{Nd}_{182}$  in the same samples (-4.8 to -5.6) is unlikely to be the result of alteration, and Fleming *et al.* (1995) concluded from

analysis of phenocryst phases, that prior to alteration, MFCT basalts must have had  $^{87}\text{Sr}/^{86}\text{Sr}_{182} \geq 0.7090$ . Alteration by the same regional hydrothermal thermal event cannot be used as an explanation for variability in the Sr-isotopic compositions of PST intrusions because the Falkland Islands would have already broken-away from the Antarctic continent by this time. In addition, the range of  $\epsilon\text{Nd}_{182}$  from -6 to -12 over the limited range of  $^{87}\text{Sr}/^{86}\text{Sr}_{182} = 0.7110$ -0.7115, for the PST intrusions, requires potential contaminants that had a range of Nd-isotopic compositions and were therefore probably of differing ages.

**Interaction with the continental lithosphere.** For the PST intrusions, the variations shown in Fig. 9 indicate that Sr- and Nd-isotopic variations were imposed on the magmas concomitant with fractional crystallization, by assimilation with fractional crystallization (AFC) or a similar process. The relationships shown in Fig. 9 require that Sr behaved incompatibly during fractional crystallization of the PST suite. The crystal cumulate formed during AFC cannot, therefore, have been plagioclase-rich. To generate the range of Sr-isotopic compositions seen in the PST intrusions requires a source with  $^{87}\text{Sr}/^{86}\text{Sr}_{182} \leq 0.7075$ , and contaminants with  $^{87}\text{Sr}/^{86}\text{Sr}_{182} > 0.7130$  and a range of  $\epsilon\text{Nd}_{182}$ , which must be  $\leq -6.0$  for all samples. Least-squares modelling of the extract and evolved liquid from a starting composition with 9.6wt% MgO (NGF16) to evolved composition with 6.78wt% MgO (MHF5.1; Table 3) requires 21% crystallization of an assemblage of orthopyroxene (74.7%), plagioclase (18.9%) and minor augite (6.4%). With only 18.9% of the fractionating assemblage being plagioclase,  $D_{\text{Sr}}$  would have been  $< 1$  which is consistent with the relationship between  $1/\text{Sr}$  and  $^{87}\text{Sr}/^{86}\text{Sr}_{182}$  in Fig. 9. In addition, Demarchi *et al.* (2001) showed that orthopyroxene is on the liquidus of Ferrar tholeiites at 1.0-1.5 GPa, suggesting that magmatic differentiation of the PST intrusions occurred at depths  $\geq 30$  km.

Sr- and Nd-isotopic compositions for PST intrusions fall in an intermediate position between the data for CT1 basalts of Dronning Maud Land and the Karoo (Fig. 12). Luttinen & Furnes (2000) argued that the extreme Nd-isotopic compositions ( $\epsilon\text{Nd}_{182} \leq -17$ ) of CT1 basalts were the

result of interaction between a mantle-derived magma and Archean (3.0 Ga) Grunehogna  
 cratonic lithosphere (Fig. 1). Riley *et al.* (2006) used AFC and energy-constrained recharge  
 AFC to model the isotopic compositions of Karoo basaltic rocks using an ORB-like source and  
 an assimilant with  $\epsilon\text{Nd}_{182} = -4$  and  $^{87}\text{Sr}/^{86}\text{Sr}_{182} = 0.710$ , and showed that the observed isotopic  
 variability in the basalts could be explained partly by these processes. In Fig. 12 three AFC  
 trajectories are plotted and the parameters used to generate the curves are given in Table 4.  
 These are not designed to fully explain the isotopic diversity in Gondwana low  $\text{TiO}_2$  continental  
 flood basalts, they have been generated in an attempt to constrain possible and impossible  
 petrogenetic processes. The starting composition has been kept constant, and is based on that of  
 largely uncontaminated low  $\text{TiO}_2$  basalts with  $\epsilon\text{Nd}_{182} = 2$  and  $^{87}\text{Sr}/^{86}\text{Sr}_{182} = 0.7035$ . For all three  
 modelled AFC trends, the ratio of the country rock assimilated to crystal cumulate formed,  $R$ ,  
 has been set at 0.40, a value that is appropriate for crystallization in the middle- to upper-crust  
 (Riley *et al.* 2006; Hole *et al.* 2015).  $D_{\text{Sr}}$  and  $D_{\text{Nd}}$  are set at 0.5 and 0.1 respectively, to simulate a  
 cumulate with approximately 25% plagioclase, and 75% ferromagnesian minerals. This means  
 that all three AFC trajectories approach the composition of the most contaminated magma for  $\leq$   
 20% AFC (Table 4). Increasing the value of  $R$  to 0.5 for any of the models does not significantly  
 change the shape of the trajectories, but decreases the amount of AFC that is needed to reach the  
 target compositions to  $\leq 12\%$ , and conversely, decreasing  $R$  to 0.3 requires  $\leq 25\%$  AFC. For the  
 CT1 AFC model, the contaminant represents 3.0 Ga Grunehogna Craton (Fig. 1) felsic granulite,  
 with  $\epsilon\text{Nd}_{182} = -50$  and  $^{87}\text{Sr}/^{86}\text{Sr}_{182} = 0.712$  (felsic xenolith sample X4-AVL of Luttinen & Furnes  
 2000). The PST-1, mixing line intersects the lowest  $\epsilon\text{Nd}_{182}$  samples in the PST suite, and the  
 contaminant represents a 2.2 Ga Palaeoproterozoic felsic granulite with  $\epsilon\text{Nd}_{182} = -20$  and  
 $^{87}\text{Sr}/^{86}\text{Sr}_{182} = 0.720$  (Luttinen & Furnes 2000). The PST-2 mixing line, which also intersects the  
 majority of data for Karoo basalts and lowest  $^{87}\text{Sr}/^{86}\text{Sr}_{182}$  ( $\sim 0.7090$ ) samples of Ferrar igneous  
 rocks, representing mixing between a mantle-derived magma and 1.0-1.5 Ga felsic crust with  
 $\epsilon\text{Nd}_{182} = -10$  and is the same contaminant as that suggested by Riley *et al.* (2006) for Karoo

basalts. Plate reconstructions place the Falkland Islands mainly within the 1.0-1.5 Ga Namaqualand-Natal-Maudheim-Mozambique belt (Thistlewood *et al.* 1997) and on the continuation of the Cape Fold Belt (Fig. 1). Mesoproterozoic crust is therefore a likely candidate for basement to the Falkland Islands, although there are no isotopic data for the Cape Meredith metamorphic complex. What is also clear is that cratonic basement like that involved in the petrogenesis of the CT1 basalts affected neither the PST intrusions nor Karoo low TiO<sub>2</sub> basaltic rocks. AFC models with geologically reasonable parameters and appropriate ages of potential basement contaminants can therefore produce the observed variations in the Sr- and Nd-isotopic characteristics of the PST intrusions for <20% AFC.

**Pyroxenite versus peridotite sources.** PST intrusions with MgO > 8 weight % have lower CaO abundances (c. 8.5 weight %) than any other of the other Falkland Islands intrusions (Figs. 4 and 13). Such compositions are uncommon in continental flood basalts provinces. Orthopyroxene was the dominant fractionating phase during crystallization of the PST (Table 3) and estimates of more primitive compositions can be calculated by incrementally adding enstatite to a mafic PST composition. Addition of 30% enstatite to sample NGF16 yields magma with ~15wt% MgO and ~7.5wt% CaO. Compositions such as these are also found in the CT1 basalts of Dronning Maud Land (Fig. 13a). An unusual feature of the PST intrusions is their Si-oversaturated nature and high Cr content (Fig. 13b) which is also reflected in unusually high Cr content of component orthopyroxene (e.g. enstatite in MHF3.2 has 0.74wt% Cr<sub>2</sub>O<sub>3</sub> at MgO/FeO = 2.8). In terms of major element compositions, PST intrusions bear strong similarities with magnesian andesite from continental subduction settings (e.g. Baker *et al.* 1994; Sato *et al.* 2014). For example, high-Mg andesites from Mt Shasta have a similar range of MgO to PST intrusions (Fig. 13a) which is accompanied by SiO<sub>2</sub> = 51.5-54.0wt%, Cr = 245-695 ppm, Ni = 99-235 ppm, TiO<sub>2</sub> = 0.6-0.8wt% and CaO = 8.6-9.6wt%. One mechanism that has been suggested for the production of high-Mg andesite is the interaction of slab-derived adakitic melts with mantle peridotite during subduction (Heinonen *et al.* 2014). A link to the previous

subduction history of the mantle source from which Ferrar and Karoo basaltic rocks were derived has been made by a number of workers (e.g. Brewer *et al.* 1992; Storey *et al.* 1992; Heinonen *et al.* 2014) and in particular, the characteristic trough at Nb and Ta relative to adjacent elements (Fig. 7) has been interpreted as an inherited subduction signature.

Herzberg & Asimow (2008) note that primary magmas derived from the melting of pyroxenite will exhibit relative CaO depletion compared to melts from a peridotite source because of the dominance of residual clinopyroxene in the source region during partial melting of pyroxenite. Given the position that data for the PST occupy in Fig. 12, it seems clear that their major element compositions are not consistent with an origin by melting of mantle peridotite. It is well established that pyroxenite can be formed at the base of the lithosphere as a result of accumulation of mafic phases during basaltic magmatism (e.g. Downes *et al.* 2007). Such accumulative pyroxenite can yield magma by partial melting at some later stage, promoted by a new phase of mafic magmatism and by interaction with peridotite-derived melts (Lambart *et al.* 2013). The generation of silica-enriched pyroxenite melts is possible, which can yield Si-oversaturated melts like those of the PST intrusions (Lambart *et al.* 2013). It is therefore suggested that the PST were derived from a pyroxenite-rich source that was emplaced at the base of the lithosphere during the prolonged subduction history of Gondwana. Metasomatism of the pyroxenite by slab-derived fluids and melt, imparted a subduction signature to the pyroxenite. When subjected to the high mantle potential temperatures associated with the mantle plume beneath Dronning Maud Land at c. 180 Ma ( $T_P$  up to 1600°C; Heinonen *et al.* 2010), the pyroxenite underwent partial melting and produced the primary melt precursor to the PST intrusions. These melts then interacted with fusible, felsic continental crust to produce the geochemical composition of the more evolved PST compositions by AFC, or a related process. Extrapolation of the MgO -  $\epsilon Nd_{182}$  trend for the PST to higher MgO contents (Fig. 9a), suggests that a primitive composition with 15 weight % MgO might have had  $\epsilon Nd_{182} \sim 0$ , and the

correlation between  $1/\text{Sr}$  and Sr-isotopic compositions requires the source to have  $^{87}\text{Sr}/^{86}\text{Sr}_{182} \leq 0.7075$ .

### ***E-W intrusions***

Least-squares modelling of the extract and evolved liquid from a starting composition ECF12 to more evolved sample ECF44 (Table 3) requires crystal fractionation of 57% olivine and 40% plagioclase feldspar with little contribution from augite (c. 2.6 %) which is a typical crystallizing assemblage for tholeiitic melts at pressures  $\leq 0.5$  GPa (e.g. Hole & Morrison 1992; Villiger *et al.* (2007), requiring E-W intrusions to have last equilibrated at  $< \sim 15$  km depth, within the crust. This is in contrast to the  $> 1.0$  GPa equilibration required by PST intrusions. The isotopic compositions of E-W intrusions require derivation from a depleted mantle source (Figs 8), but they have higher Th/Ta (2.2-2.8) and La/Ta (16.4-26.1) than would be expected if they were derived from asthenospheric mantle (Th/Ta  $\sim 1.0$  and La/Ta  $\leq 18$ ; Sun & McDonough 1989) and they also exhibit a noticeable trough at Nb and Ta relative to adjacent elements in Fig. 7, a feature that is most often attributed to interaction with continental lithosphere. However, the extent of this interaction must either have been limited, or the source from which the E-W intrusions were derived had a Th/Ta  $> 2.0$  and La/Ta  $> 26$ . The low pressure equilibration of E-W intrusions, coupled with their depleted isotopic compositions may suggest that they were emplaced during a period of crustal attenuation and were thus able to escape interaction with continental lithosphere.

### ***DIT and Lively Island intrusions***

In contrast to the PST intrusions, the sub-horizontal arrays delineated by DIT intrusions in Fig. 9a, suggests that AFC or a similar process was not important during their petrogenesis. However, a negative correlation between Th/Ta and  $\epsilon\text{Nd}_{182}$  for the DIT intrusions (Fig. 9b) may require minor modification by a crustal component with Th/Ta  $\geq 3.0$ . A characteristic feature of the DIT samples is that they have  $\epsilon\text{Nd}_{182}$  in range -2.8 to +0.6, but with only a single analysed sample (NHF17) having  $\epsilon\text{Nd}_{182} < -1$ . In addition, the Lively Island dyke, which falls close to the

fractionation trend for the MFCT basaltic rocks of the Transantarctic Mountains (Fig. 11), has Sr- and Nd-isotopic compositions ( $^{87}\text{Sr}/^{86}\text{Sr}_{182}$  c. 0.7052,  $\epsilon\text{Nd}_{182} = -0.5$  to  $-1.4$ ) that do not require the significant isotopic enrichment seen in the Ferrar dolerites ( $\epsilon\text{Nd}_{182}$  in the range  $-3.3$  to  $-5.3$ ; Fleming *et al.* 1995; Hergt *et al.* 1989). The source of the low  $\text{TiO}_2$  DIT magmas could, therefore, have had  $\epsilon\text{Nd}_{182} > 0$ ,  $^{87}\text{Sr}/^{86}\text{Sr}_{182} < 0.7050$ ,  $\text{Th}/\text{Ta} < 2.5$  and  $\text{La}/\text{Ta} < 20$ .

### ***MAT intrusions***

The positive  $\epsilon\text{Nd}_{182}$  (2.7-3.6) and low  $\text{Th}/\text{Ta}$ ,  $\text{La}/\text{Ta}$  and  $[\text{La}/\text{Yb}]_N$  (0.8-1.0; 12.8-17.3 and 1.9-3.7 respectively) of MAT intrusions suggests that they were derived from an asthenospheric source, and escaped significant interaction with lithosphere. The most satisfactory explanation for the geochemical compositions of these rocks is that they were generated by decompression melting of the asthenosphere during the rifting stage of Gondwana break-up. In this respect they have similar geochemical compositions to the ORB-like Rooi Rand basaltic dykes of the southern Lebombo (Cox & Bristow 1984, which post-date the main magmatic phases in the region by about 5 Myr (Jourdan *et al.* 2007).

### ***Cretaceous intrusions***

Until more data are forthcoming, the origin and affinity of the Cretaceous Teal Creek intrusion reported by Stone *et al.* (2009) remains somewhat obscure. Major element data for the intrusion plot close to the Theron Mountains low  $\text{TiO}_2$  trend in Fig. 6, but the intrusion has higher  $\text{Fe}_2\text{O}_3$  (c. 15.9wt%) at 5.7wt%  $\text{MgO}$  than any of the data for the intrusions presented here. What is clear, is that there is an extensive suite of low  $\text{TiO}_2$  basalts within the Etendeka Province (e.g. Gibson *et al.* 2005; Thompson *et al.* 2001) from which it could be related. However, none of the groups of intrusions described here carries a similar signature to that presented by Stone *et al.* (2009) for the Teal Creek dyke.

## **Provinciality and chemical affinities of Falkland Islands intrusions**



A number of authors have noted that there are spatially constrained variations in major and trace element compositions within the Jurassic Gondwana break-up related flood basalts provinces of the Southern Hemisphere (e.g. Brewer *et al.* 1992; Luttinen & Furnes 2000; Riley *et al.* 2006). Figs 11 and 14 illustrate the variability in abundances of MgO, TiO<sub>2</sub>, SiO<sub>2</sub> and Ti/Zr for Falkland Island intrusions, along with igneous rocks which are defined as being either Karoo or Ferrar magma types, or those which are considered to be transitional between the two magma types (Brewer *et al.* 1992; Luttinen & Furnes 2000; Riley *et al.* 2006). In the following sections, we will examine the geochemical affinities of the Falklands Islands intrusions in relationship to other early Jurassic flood basalts of Gondwana.

#### ***PST intrusions***

PST intrusions exhibit strong similarities to CT1 basalts of Dronning Maud Land (e.g. Fig. 14), and show some overlap with the compositional field for samples from the Theron Mountains and Transantarctic Mountains. In terms of incompatible trace elements, PST dykes exhibit almost identical multi-elements patterns to sample SA.6.1 (Fig. 7; Riley *et al.* 2006) from KwaZulu-Natal, with which they share also unradiogenic Nd-isotopic compositions (e.g. SA.6.1  $\epsilon_{\text{Nd}_{182}} = -8.9$ ). Within the CT1 basalts of Dronning Maud Land, very similar compositions to PST intrusions can be found (e.g. B70-AVL; Luttinen & Furnes 2000) again with many basalts in the CT1 suite having unradiogenic Nd-isotopic compositions (Fig. 12). Furthermore, both CT1 and PST magmas required derivation from a pyroxenite-rich, CaO deficient, source region (Fig. 13). It is with some confidence that we conclude that the PST, CT1 and some KwaZulu-Natal basalts were derived from very similar source regions, had similar petrogenetic histories and represent the same phase of pre-break-up magmatism.

#### ***E-W intrusions***

These igneous rocks exhibit a strong geochemical affinity with basalts from Kirwanveggan (Harris *et al.* 1990) and Schirmaker Oasis (Sushchevskaya *et al.* 2009), Dronning Maud Land (Figs 11 and 14). A notable characteristic of all the above samples is that they have radiogenic

Nd-isotopic compositions ( $\epsilon\text{Nd}_{182} = 2-6$ )  $^{87}\text{Sr}/^{86}\text{Sr}_{182}$  in the restricted range 0.7040-0.7060 and  $^{206}\text{Pb}/^{204}\text{Pb}$  in the range 17.97-18.49 and plot close to the NHRL in Fig. 8. These isotopic characteristics, coupled with  $\text{Ti}/\text{Zr} = 70-90$  and  $\text{SiO}_2 = 47.0-52.8\text{wt\%}$ , clearly separates Kirwanveggan, Schirmaker Oasis and Falkland Islands E-W intrusions from PST intrusions. E-W intrusions also fall within the compositional field for basalts from the Central Karoo of South Africa in Fig. 14, and intrusions with compositions similar to those of Falkland Islands E-W intrusions are prevalent in the Golden Valley Sill Complex (Neumann *et al.* 2011).

#### ***DIT and Lively Island intrusions***

In Fig. 14b, DIT intrusions exhibit almost complete overlap with the MFCT Ferrar dolerites of the Transantarctic Mountains. However, consideration of Fig. 11, shows that DIT intrusions are not of the same low  $\text{TiO}_2$  ( $<0.5-1.2\text{wt\%}$ ) lineage of the MFCT. However, DIT intrusions do have compositions that overlap with those for low  $\text{TiO}_2$  Theron Mountains basalts and samples from KwaZulul-Natal that Riley *et al.* (2006) and Brewer *et al.* (1992) argued were transitional between Ferrar and Karoo magma types. We concur with this hypothesis, and given the position that the Falkland Islands occupied in southern Gondwana at the time of Karoo and Ferrar magmatism, this seems entirely reasonable.

The Lively Island intrusion is the only member of the intrusive suite of rocks of the Falkland Islands that falls within the compositional range for MFCT samples from the Transantarctic Mountains in Figs 11 and 14. However, the Lively Island intrusion has considerably lower  $\text{La}/\text{Ta}$  and  $\text{Th}/\text{Ta}$  (20.5 and 3.2 respectively) than the majority of the MFCT dolerites ( $\text{La}/\text{Ta}$  19-47;  $\text{Th}/\text{Ta}$  4.3-23.3), and the Lively Island dyke also has considerably more radiogenic Nd ( $\epsilon\text{Nd}_{182} = -0.5$  to  $-1.4$ ) than MFCT dolerites ( $\epsilon\text{Nd}_{182} = -4.7$  to  $-5.7$ ). It is important to note, that the Lively Island intrusion is a single body of igneous rock around 30m thick, and consequently is not a volumetrically significant part of the Falkland Islands dyke swarm.

#### ***MAT intrusions***

Ti/Zr>90 coupled with SiO<sub>2</sub> of 45.7-51.0wt% are characteristics that MAT intrusions share with CT2 and CT3 basalts from Dronning Maud Land and samples from the Rooi Rand dyke swarm of the southern Lebombo area of southern Africa (Cox & Bristow 1984). The unradiogenic Sr-isotopic compositions (<sup>87</sup>Sr/<sup>86</sup>Sr<sub>182</sub> c. 0.7040) and radiogenic Nd-isotopic compositions (εNd<sub>182</sub> = 2.5-4.0) of E-W intrusions also characterize Rooi Rand and CT2 and CT3 basalts, although the Dronning Maud Land samples have a rather more extended range of isotopic compositions, which Luttinen & Furnes (2000) attribute to conservative amounts of interaction with upper-crustal felsic contaminants.

### **Mantle potential temperature, rifting and magmatism**

Fig. 15a summarizes the available data for olivine equilibration temperatures (T<sub>OL</sub>) for MAT and E-W basalts and picrites from Dronning Maud. MAT and E-W basalts yield olivine equilibration temperatures of 1245°C and 1330°C respectively, using the method of Putirka *et al.* (2007), whilst olivine in picrites from Dronning Maud Land yield T<sub>OL</sub> up to 1450°C. Converting equilibration temperatures to T<sub>P</sub> is problematical if the pressure and extent of melting cannot be independently determined (Herzberg & Asomow 2008; Herzberg & Gazel 2009; Hole 2015), which they cannot for the MAT and E-W samples. However, since olivine equilibration temperature increases with increasing pressure of crystallization, synthetic olivine liquids can be calculated for any given temperature and pressure (Herzberg & Gazel 2009). Fig. 15b shows the inferred temperature-pressure conditions at which fractional melting terminated for calculated primary magmas from Dronning Maud Land, the Karoo Province of southern Africa, Ferrar dolerites of Antarctica. (Hole 2015). In Fig. 15c, data for basalts from the Cretaceous Etendeka Province of SW Africa (Kieding *et al.* 2011) are given, for which estimates of T<sub>OL</sub>, estimates of T<sub>P</sub> from melt inclusions in ultra-magnesian olivine, and estimates of T<sub>P</sub> from the PRIMEL2 model of Herzberg & Asimow (2008) have all been calculated on the same samples. Using the Herzberg & Asimow (2008) model yields T<sub>P</sub> = 1500-1550°C and final pressures of melting (P<sub>f</sub>) between 1.5 and 4.0 GPa (Fig. 13c). T<sub>P</sub> from melt inclusions is 1300-

1520°C, whilst  $T_{OL}$  is in the range 1250-1400°C and there is an empirical relationship between  $T_{OL}$  and melt inclusion  $T_P$  which approximates to  $T_P = 1.443 \times T_{OL} - 501$  for the Etendeka plume system (Fig. 15). Therefore it seems that within a single plume system, basalts may be generated over ranges of  $T_P$  that are larger than the  $\pm 50^\circ\text{C}$  error inherent in the calculation methods (Herzberg & Asimow 2009; Hole 2015). Direct application of this empirical observation to the Dronning Maud Land picrites suggest maximum  $T_P \sim 1550^\circ\text{C}$ , a temperature that is considered to be associated with ‘hot’ mantle plumes such as Iceland at 60 Ma (Fig. 15; Herzberg & Gazel 2009). For Falkland Islands E-W basalts,  $T_{OL} \sim 1330^\circ\text{C}$ , which implies  $T_P \sim 1400^\circ\text{C}$  and for olivine-phyric MAT basalts,  $T_{OL} \sim 1250^\circ\text{C}$  implying  $T_P \sim 1300^\circ\text{C}$ . These  $T_P$  estimates for the Falkland Islands E-W and MAT basalts may therefore be reconciled with a model involving melting of mantle with near-ambient temperature ( $T_P \geq 1350^\circ\text{C}$ ), but would require intersection of the dry peridotite solidus at  $\sim 2.1$  GPa ( $\sim 70\text{km}$ ) and all melting to take place in the spinel stability field of the mantle; the most mafic MAT and E-W intrusions have  $[\text{La/Yb}]_N < 2.0$  which does not preclude such an origin. Additionally, near-ambient  $T_P$  melting would require the continental lithosphere to be thinned substantially and perhaps to  $< 50\text{km}$ , to allow decompression melting to take place. The depleted isotopic compositions of the E-W and MAT intrusions, along with the  $< 0.5$  GPa equilibration of the E-W magmas, provides additional evidence to suggest that these intrusions were emplaced during a period of crustal stretching, possible coeval with the initiation of Gondwana. Nevertheless, whilst there is no primary evidence to suggest  $T_P$  was  $> 1450^\circ\text{C}$  beneath the Falkland Islands at 180 Ma, it is possible that high-MgO large melt fractions requiring substantially higher  $T_P$  exist in the region, but have not been sampled, remains a possibility.

The diversity of magma types found in the Falkland Islands, and the position in Gondwana which the islands occupied during magmatism (Fig. 1) is entirely consistent with their being close to the focus of magmatism during continental break-up. We concur with Brewer *et al.* (1992) and Riley *et al.* (2006) that there is considerable overlap in the geographical distribution

of the Ferrar and Karoo LIPs, which is most obvious in the Theron Mountains and Falkland Islands. It is also clear, that despite the wealth of geochemical data available for the Transantarctic Mountains and Tasmania, there is no evidence to suggest that volcanic rocks with affinities to the Karoo LIP occur in those areas. With the exception of the ORB-like basalts of the Rooi Rand dyke swarm (Marsh *et al.* 1997; Mitchell *et al.* 1999) which are likely to represent syn-break-up magmas, basaltic rocks with Karoo-type geochemical compositions only extend as far south as the overlap zone in the Theron Mountains.

## Conclusions

The Jurassic (c. 182 Ma) intrusions of the Falkland Islands exhibit a broad range of geochemical compositions and at least four main petrogenetic lineages are recognized. PST intrusions were derived by melting of an isotopically-enriched pyroxenite-rich source, followed by orthopyroxene-dominated crystal fractionation at  $\geq 1$  GPa. Pyroxenite-derived PST magmas subsequently interacted with ‘old’ ( $\geq 2.2$  Ga) fusible continental lithospheric components by AFC or a related process. The geochemical compositions of DIT intrusions bear striking similarities to igneous rocks of Kwazulu-Natal and the Theron Mountains, which are considered to be transitional in composition between those of the Ferrar and Karoo magma types. A significant number of mafic (Mg# 50-62) E-W and MAT intrusions possess radiogenic Nd- and unradiogenic Sr-isotopic compositions ( $^{87}\text{Sr}/^{86}\text{Sr}_{182} < 0.7050$  and  $\epsilon\text{Nd}_{182} > 2.5$ ), also have Th/Ta and La/Ta ( $< 3.0$  and  $< 25$  respectively) that require little input from the continental lithosphere. In addition, E-W intrusions carry mineralogical and chemical fingerprints of equilibration at  $< 0.5$  GPa. E-W and MAT basalts were probably emplaced during rifting and continental break-up and are likened to the Rooi Rand dykes of the Southern Lebombo of Africa. However, there is currently no evidence to suggest that the Falkland Islands intrusions were derived by melting above a significant mantle thermal anomaly. Early Jurassic plate reconstructions place the Falkland Islands close to the Weddell Triple Junction, perhaps explaining the diversity of igneous rock compositions found in a relatively limited geographical region.

514 **Acknowledgements.**

515 An earlier version of the manuscript was improved by thoughtful comments from two  
516 anonymous reviewers. Dr D. Aldis, Falkland Islands Geological Survey, is thanked for  
517 providing some samples from Fox Bay West for this study.

518

## References Cited.

- Antonini, P., Piccirillo, E.M., Petrini, R., Civetta, M., D'Antonio, M. & Orsi, G. 1999. Enriched mantle Dupal signature in the genesis of the Jurassic Ferrar tholeiites from the Prince Albert Mountains, (Victoria Land, Antarctica). *Contributions to Mineralogy and Petrology*, **136**, 1-19.
- Baker, M.B., Grove, T.L. and Price, R.C. 1994. Primitive basalts and andesites from the Mt. Shasta region, N. California: products of varying melt fraction and water content. *Contributions to Mineralogy and Petrology*, **118**, 111-129.
- Brewer, T. S., Hergt, J. M., Hawkesworth, C. J., Rex D. C. & Storey B. C. 1992. Coats Land dolerites and the generation of Antarctic continental flood basalts. *In: Storey, B. C., Alabaster, T. & Pankhurst, R. J. (eds) Magmatism and the causes of Continental Break-Up* Geological Society, London, Special Publications, **64**, 185-208.
- Burgess, S.D., Bowring, S.A., Fleming, T.H. & Elliot, D.H. 2015. High-precision geochronology links the Ferrar large igneous province with early-Jurassic ocean anoxia and biotic crisis. *Earth and Planetary Science Letters*, **415**, 90-99.
- Coltice, N., Bertrand, H., Rey, P.M., Jourdan, F., Phillips, B.R. & Ricard, Y. 2009. Global warming of the mantle beneath continents back to the Archaean. *Gondwana Research*, **15**, 254-266.
- Cox, K.G. & Bristow, J.W. 1984. The Sabine River Basalt Formation of the Lebombo Monocline and south-east Zimbabwe. *In: Petrogenesis of the volcanic rocks of the Karoo province*, A.J. Erlank (ed). Special Publication of the Geological Society of South Africa, **13**, 124-147.
- Demarchi, G., Antonini, P., Piccirillo, E.M., Orsi, G., Civetta, L. & D'Antonini, M. 2001. Significance of orthopyroxene and major element constraints on the petrogenesis of Ferrar tholeiites from southern Prince Albert Mountains, Victoria Land, Antarctica. *Contributions to Mineralogy and Petrology*, **142**, 127-146.
- Downes, H., Upton, B.G.J., Connolly, J., Beard, A.D. & Bodinier, J-L 2007. Evidence for late Palaeozoic crustal underplating beneath SW Scotland Petrology and geochemistry of a cumulate xenolith suite from Bute. *Journal of the Geological Society, London*, **164**, 1217-1231.
- Elliot, D.H. 2013. The geological and tectonic evolution of the Transantarctic Mountains: a review. *In: Hambrey, M.J., Barker, P.F., Barrett, P.J., Bowman, V., Davies, B., Smellie, J.L. & Tranter, M (eds). Antarctic Palaeoenvironments and Earth-surface process.* Geological Society London, Special Publications, **381**, 7-35.



553 Elliot, D. H. & Fleming, T. H. 2000. Weddell Triple Junction: The principal focus of Ferrar and  
 554 Karoo magmatism during the initial break-up of Gondwana. *Geology*, **28**, 539-542.

555 Elliot, D. H. & Fleming, T. H. 2004. Occurrence and Dispersal of Magmas in the Jurassic Ferrar  
 556 Large Igneous Province, Antarctica. *Gondwana Research*, B, 223-237.

557 Elliot, D.H., Fleming, T.H., Haban, M.A. & Siders, M.A. 1995. Petrology and mineralogy of the  
 558 Kirkpatrick Basalt and Ferrar Dolerite, Mesa Region, Northern Vitoria Land, Antarctica. *In*:  
 559 Elliot, D.H. & Blaisdell, L.L. (eds) *Contribution to Antarctic Research IV*. Antarctic  
 560 Research Series, 67. American Geophysical Union, Washington DC, 103-141.

561 Elliot, D. H., Fleming, T. H., Kyle, P. R. & Foland, K. A. 1999. Long-distance transport of  
 562 magmas in the Jurassic Ferrar large igneous province, Antarctica. *Earth and Planetary  
 563 Science Letters*, **167**, 89–104.

564 Fleming, T.H., Foland, K.A. & Elliot, D.H. 1995. Isotopic and chemical constraints on the  
 565 crustal evolution and source signature of Ferrar magmas, north Victoria Land, Antarctica.  
 566 *Contributions to Mineralogy and Petrology*, **121**, 217-236.

567 Galerne, C.Y., Nuemann, E-R. & Planke, S. 2008. Emplacement mechanisms of sill complexes:  
 568 Information from the geochemical architecture of the Golden Valley Sill Complex, South  
 569 Africa. *Journal of Volcanology and Geothermal Research*, **177**, 425-440.

570 Gibson, S.A., Thompson, R.N., Day, J.A., Humphris, S.E. & Dickin A.P. 2005. Melt-generation  
 571 associated with the Tristan mantle plume: constraints on the origin of EM-1. *Earth and  
 572 Planetary Science Letters*, **237**, 744-767.

573 Greenway, M. E., 1972. The geology of the Falkland Islands. *British Antarctic Survey Scientific  
 574 Reports*, **76**, 42 pp.

575 Harris, C., Marsh, J.S., Duncan, A.R. & Erlank, A.J. 1990. The Petrogenesis of the Kirwan  
 576 Basalts of Dronning Maud Land, Antarctica. *Journal of Petrology*, **31**, 341-369.

577 Heinonen, J.S. & Luttinen, A.V. 2008. Jurassic dikes of Vestfjella, western Dronning Maud  
 578 Land, Antarctica: Geochemical tracing of ferropicrite sources. *Lithos*, **105**, 347-364.

579 Heinonen, J.S., Carlson, R.W. & Luttinen, A.V. 2010. Isotopic (Sr, Nd, Pb, and Os) composition  
 580 of highly magnesian dikes of Vestfjella, western Dronning Maud Land, Antarctica: A key to  
 581 the origins of the Jurassic Karoo large igneous province? *Chemical Geology*, **277**, 227-244.

582 Heinonen, J.S., Luttinen, A.V., Riley, T.R. & Nichallik, R.M. 2013. Mixed pyroxenite–  
 583 peridotite sources for mafic and ultramafic dikes from the Antarctic segment of the Karoo  
 584 continental flood basalt province. *Lithos*, **177**, 266-380.

- Heinonen, J.S., Carlson, R.W., Riley, T.R., Luttinen, A.V. & Horan, M.F. 2014. Subduction-modified oceanic crust mixed with a depleted mantle reservoir in the sources of the Karoo continental flood basalt province. *Earth and Planetary Science Letters*, **394**, 229-241.
- Hergt J. M., Chappell B. W., Mcculloch M. T., McDougall I. & Chivas A. R. 1989. The geochemistry of Jurassic dolerites from Portal Peak, Antarctica. *Contributions to Mineralogy and Petrology*, **102**, 298-305.
- Herzberg, C. & Asimow, P.D. 2008. Petrology of some oceanic island basalts: PRIMELT2.XLS software for primary magma calculation. *Geochemistry, Geophysics, Geosystems*, **9**.
- Herzberg, C. & Gazel, E. 2009. Petrological evidence for secular cooling in mantle plumes. *Nature*, **458**, 619-623.
- Hole, M.J. 2015. The generation of continental flood basalts by decompression melting of internally heated mantle. *Geology*, **43**, 311-314.
- Hole M.J. & Morrison, M.A. 1992. The differentiated boss Cnoc Rhaonastil, Islay; a natural experiment in the low pressure differentiation of an alkali olivine-basalt magma. *Scottish Journal of Geology*, **28**, 55-69.
- Hole, M.J., Millett, J.M., Rogers, N.W. & Jolley, D.W. 2015. Rifting and mafic magmatism in the Hebridean basins. *Journal of the Geological Society, London*, **172**, 218-236.
- Jourdan F., Bertrand H., Schärer U., Blichert-Toft J., Feraud G. & Kampunzu A.B. 2007b. Major and trace element and Sr, Nd, Hf, and Pb isotope compositions of the Karoo large igneous province, Botswana-Zimbabwe: lithosphere vs mantle plume contribution. *Journal of Petrology*, **48**, 1043-1077.
- Keiding, J.K., Trumbull, R.B., Veksler, I.V. & Jerram, D.A. 2011. On the significance of ultra-magnesian olivines in basaltic rocks. *Geology*, **39**, 1095-1098.
- Lambart, S., Lapporte, D. & Schiano, P. 2013. Markers of the pyroxenite contribution in the major-element compositions of oceanic basalts: Review of the experimental constraints. *Lithos*, **160-161**, 14-36.
- Luttinen, A.V. & Furnes, H., 2000. Flood basalts of the Vestfjella: Jurassic magmatism across an Arcehan-Proterozoic lithospheric boundary in Dronning Maud Land, Antarctica. *Journal of Petrology*, **41**, 1271-1305.
- Luttinen, A.V., Ramo, O.T. & Huhma, H. 1998. Neodymium and strontium isotope and trace element composition of a Mesozoic CFB suite from Dronning Maud Land, Antarctica: implications for lithosphere and asthenosphere contributions to Karroo magmatism. *Geochimica et Cosmochimica Acta*, **15**, 2701-2714.

- 618 Macdonald, D.I.M., Gomez-Perez, I., Franzese, J., Spalletti, L., Lawver, L., Gahagan, L.,  
619 Dalziel, I.W.D., Thomas, C.J., Trewin, N.H., Hole, M.J. & Paton, D. 2003. Mesozoic break-  
620 up of SW Gondwana: implications for regional hydrocarbon potential of the southern South  
621 Atlantic. *Marine & Petroleum Geology*, **20**, 287-308
- 622 Marsh, J.S., Hooper, P.R., Rehacek, J., Duncan, R.A. & Duncan, A.R. 1997. Stratigraphy and  
623 age of Karroo basalts of Lesotho and implications for correlations within the Karroo  
624 Igneous Province. In: Mahoney, J.J. & Coffin, M.F. (eds) *Large Igneous Provinces*, A G U  
625 Geophysical Monographs, 100, 247-272.
- 626 McClintock, M., Marsh, J. & White, J.D.L. 2008. Compositionally diverse magmas erupted  
627 close together in space and time within a Karroo flood basalt crater complex. *Bulletin of*  
628 *Volcanology*, **70**, 923-946.
- 629 Mitchell, C., Ellam, R.M. & Cox, K.G. 1999. Mesozoic dolerite dykes of the Falkland Islands:  
630 petrology, petrogenesis and implications for geochemical provinciality in Gondwanaland  
631 low-Ti basaltic rocks. *Journal of the Geological Society, London*, **156**, 901-916.
- 632 Molzahn, M., Reisberg, L. & Wörner, G. 1996. Os, Sr, Nd, Pb, O isotope and trace element  
633 data from the Ferrar flood basalts, Antarctica: evidence for an enriched subcontinental  
634 lithospheric source. *Earth and Planetary Science Letters*, **144**, 529-546.
- 635 Muirhead, J.D., Airoidi, G., White, J.L. and Rowland, J.V. 2014. Cracking the lid: Sill-fed  
636 dikes are the likely feeders of flood basalt eruptions. *Earth and Planetary Science Letters*,  
637 **406**, 187-197.
- 638 Mussett, A.E. & Taylor, G.K. 1994.  $^{40}\text{Ar}$ - $^{39}\text{Ar}$  ages for dykes from the Falkland Islands with  
639 implications for the break-up of southern Gondwanaland. *Journal of the Geological Society*,  
640 *London*, **151**, 79-81.
- 641 Nuemann, E-R., Svensen, H., Galerne, G.Y. & Planke, S. 2011. Multistage Evolution of  
642 Dolerites in the Karroo Large Igneous Province, Central South Africa. *Journal of Petrology*,  
643 **52**, 959-984.
- 644 Putirka, K.D., Perfit, M., Ryerson, F.J. & Jackson, M.G. 2007. Ambient and excess mantle  
645 temperatures, olivine thermometry, and active vs. passive upwelling. *Chemical Geology*, **241**,  
646 177-206.
- 647 Richards, P.C., Stone, P., Kimbell, G.S., McIntosh, W.C. & Phillips, E.R. 2013. Mesozoic  
648 magmatism in the Falkland Islands (South Atlantic) and their offshore sedimentary basins.  
649 *Journal of Petroleum Geology*, **36**, 61-74.

- Riley, T.R., Curtis, M.L., Leat, P.T., Watkeys, M.K., Duncan, R.A., Millar, I.L. & Owens, W.H. 2006. Overlap of Karoo and Ferrar Magma Types in KwaZulu-Natal, South Africa. *Journal of Petrology*, **47**, 541-566.
- Sato, M., Shuto, K., Nohara-Imanaka, R., Takazawa, E., Osanai, Y. & Nakano, N. 2014. Repeated magmatism at 34 Ma and 23-20 Ma producing highmagnesian adakitic andesites and transitional basalts on southern Okushiri Island, NE Japan arc. *Lithos*, **205**, 60-83.
- Sushchevskaya, N.M., Korago, E.A., Belyatsky, B.V. & Sirotkin, A.N. 2009. Evolution of the Karoo-Maud mantle plume in Antarctica and its influence on the magmatism of the early stages of Indian ocean opening. *Geochemistry International*, **47**, 1-17.
- Stone, P., Kimbell, G.S. & Richards, P.C. 2009. Rotation of the Falklands microplate reassessed after recognition of discrete Jurassic and Cretaceous dyke swarms. *Petroleum Geoscience*, **15**, 279-287.
- Stone, P., Richards, P.C., Kimbell, G.S., Esser, R.P., & Reeves, D. 2008 Cretaceous dykes discovered in the Falkland Islands: implications for regional tectonics in the South Atlantic. *Journal of the Geological Society, London*, **165**, 1-4
- Storey, B.C., Alabaster, T., Hole, M.J., Pankhurst, R.J. & Wever, H. 1992. Role of subduction-plate boundary forces during the initial stages of Gondwana break-up: Evidence from the proto-Pacific margin of Antarctica. In: Storey, B. C., Alabaster, T. & Pankhurst, R. J. (eds) *Magmatism and the causes of Continental Break-Up* Geological Society, London, Special Publications, **64**, 149-163.
- Sweeney R. J., Duncan A. R., Erlank A. J. 1994. Geochemistry and Petrogenesis of Central Lebombo basalts of the Karoo igneous province. *Journal of Petrology*, **35** 95-125.
- Sun, S-S. & McDonough, W. F. 1989. Chemical and isotopic systematics of oceanic basalts: implications for mantle composition and processes. In: Saunders, A.D. & Norry, M.J., (eds). *Magmatism in the ocean basins*. Geological Society, London, Special Publications, **42**, 313-345.
- Sushchevskaya, N. M., Belyatskii, B. V., Leichenov, G. L. & Laiba A. A. 2009. Evolution of the Karoo-Maud plume in Antarctica and its influence on the magmatism of the early stages of Indian Ocean opening. *Geochemistry International*, **47**, 1-17
- Svensen, H., Corfu, F., Polteau, S., Hammer, O & Planke, S. 2012. Rapid magma emplacement in the Karoo Large Igneous Province. *Earth and Planetary Science Letters*, **325-326**, 1-9.
- Thistlewood, L., Leat, P. T., Millar, I.L., Storey, B.C. & Vaughan, A. P. M. 1997. Basement Geology and Palaeozoic-Mesozoic mafic dykes from the Cape Meredith Complex, Falkland

- Islands: a record of repeated intracontinental extension. *Geological Magazine*, **134**, 355-367.
- Thompson, R.N., Gibson, S.A., Dickin, A.P. & Smith, P.M. 2001. Early Cretaceous basalt and picrate dykes of the Southern Etendeka region, NW Namibia: windows into the role of the Tristan plume in Parana-Etendeka magmatism. *Journal of Petrology*, **42**, 2049-2081.
- Trewin, N.H., Macdonald, D.I.M., & Thomas, C.G.C. 2002. Stratigraphy and sedimentology of the Permian of the Falkland Islands: lithostratigraphic and palaeoenvironmental links with South Africa. *Journal of the Geological Society, London*, **159**, 5–19.
- Villiger, S., Ulmer, P. & Muntener, O. 2007. Equilibrium and fractional crystallization experiments at 0.7 GPa; the effect of pressure on phase relations and liquid compositions of tholeiitic magmas. *Journal of Petrology*, **48**, 159-184.
- Wilhelm, S. & Wörner, G. 1996. Crystal size distribution in Jurassic Ferrar flows and sills (Victoria Land, Antarctica): evidence for processes of cooling, nucleation and crystallization. *Contributions to Mineralogy and Petrology*, **125**, 1-15.
- Williamson, I.T. & Bell, B.R. 2012. The Staffa Lava Formation: graben-related volcanism, associated sedimentation and landscape character during the early development of the Palaeogene Mull Lava Field, NW Scotland. *Scottish Journal of Geology*, **48**, 1-46.

## Figure Captions

Figure 1. a) Reconstruction of Southern Gondwana showing the position of the Falkland Islands relative to south-eastern Africa prior to continental break-up. The three arrows represent the main dyke trends on the Falkland Islands rotated back to their pre-180 Ma orientation. After Trewin *et al.* (2002). b) Southern Gondwana, in the Middle Jurassic, showing the distribution of Jurassic break-up related magmas in southern Africa and Antarctica. MEB, Maurice Ewing Bank; EWM, Ellsworth-Whitmore Mountains; AP, Antarctic Peninsula; SA, South Africa; SAM, South America; ANT, Antarctica. Position of the Weddell, Limpopo and Lower Zambesi triple junctions are from Elliot & Fleming (2000). Ar-Ar ages, this study and Stone *et al.* (2009). After Macdonald *et al.* (2003). Key to shading for Fig. 1b is the same as that for Fig. 1a.

Figure 2. Map of the Falkland Islands showing the distribution of magnetic anomalies and main trends of dyke swarms. Solid or pecked lines do not necessarily represent continuous exposure of dykes. Inset; azimuths of Dykes in the South Harbour area of West Falkland. The rectangle at South Harbour is the area covered by the map in the supplementary material, which gives the sample locations and geochemical type to which the dykes belong in that area. After Stone *et al.* (2009) and Richards *et al.* (2013). Ar-Ar ages (this study, Stone *et al.* 2008; 2009) and sample locations which are mentioned in the text, are indicated, along with the geochemical group to which the intrusions belong, given by the following abbreviations; PST, Port Sussex Type; MAT, Mount Alice Type, E-W, East-West Type of Mitchell *et al.* (1999); DIT, Dyke Island Type. Identifying characteristics of each type of intrusion are discussed in detail in the text.

Figure 3. Ar-Ar step-heating spectrum for plagioclase in sample WI-5. Full data are given in the supplementary materials.

Figure 4. Major (wt%) and trace element (in ppm) variations *versus* MgOwt% in Falkland Islands dykes. Filled dots, Port Sussex Creek type (PST) NE-SW two-pyroxene dolerites; open triangles, E-W olivine dolerite dykes; open squares, Lively Island dyke; filled squares, Mount Alice-type (MAT) dykes; open dots, low TiO<sub>2</sub> DIT intrusions; filled diamonds, high TiO<sub>2</sub> DIT intrusions; open diamonds, evolved sheets from the South Harbour-Dyke Island transect (Dyke Island Type; DIT); crosses, Pony's Pass N-S Cretaceous dyke (Stone *et al.* 2008). Data from this study, Mitchell *et al.* (1999) and Thistlewood *et al.* (1997).

Figure 5. Pyroxene end-member compositions represented in the quadrilateral system Enstatite - Ferrosilite – Wollastonite for Falkland Islands intrusions (this study and Mitchell *et al.* 1999) and dolerites from the Transantarctic Mountains (Elliot 1995; Demarchi *et al.* 2001). MFCT,

Mount Fazio Chemical Type; SPCT, Scarab Peak Chemical Type; NVL, Northern Victoria Land.

Figure 6. Chondrite-normalized REE profiles for representative samples of a) DIT intrusions and b) PST, MAT and E-W intrusions.

Figure 7. a) to d) Multi-element ORB-normalized (Sun & McDonough 1989) variation diagrams for Falkland Islands dykes. Comparable basalts from other regions of the low TiO<sub>2</sub> Gondwana LIP are shown by grey lines. Sample SA.6.1 (South Africa), Riley *et al.* (2006); VF111-85, CT3 basalt, Dronning Maud Land (Luttinen & Furnes 2000); 47206-3, low TiO<sub>2</sub> tholeiite from Schirmacher Oasis, Dronning Maud Land (Sushchevskaya *et al.* 2009); Average MFCT from Elliot *et al.* (1995).

Figure 8. a)  $\epsilon\text{Nd}_{182}$  versus  $^{87}\text{Sr}/^{86}\text{Sr}_{182}$ ; b)  $^{207}\text{Pb}/^{204}\text{Pb}$  versus  $^{206}\text{Pb}/^{204}\text{Pb}$  for Falkland Islands dykes. c)  $\epsilon\text{Nd}_{182}$  versus  $^{207}\text{Pb}/^{204}\text{Pb}$  for Falkland Islands intrusions. Symbols as for Fig. 4. Data sources this study, Mitchell *et al.* (1999) and Thistlewood *et al.* (1997).

Figure. 9 a)  $\epsilon\text{Nd}_{182}$  versus MgO; b)  $\epsilon\text{Nd}_{182}$  versus Th/Ta and c)  $^{87}\text{Sr}/^{86}\text{Sr}_{182}$  versus 1/Sr for Falkland Islands intrusions. Symbols as for Fig. 4 except grey dots are for the lowest reported Th/Ta for Ferrar dolerites (Fleming *et al.* 1995). Parameters for the AFC mixing line are given in Table 4 with % AFC given on the mixing line.

Figure 10. Ti/Zr versus SiO<sub>2</sub> for Falkland Islands dykes. Symbols as for Fig. 4.

Figure 11. TiO<sub>2</sub> versus MgO, for Falkland Islands dykes the Ferrar LIP and igneous rocks considered to be transitional between the compositions of Ferrar and Karoo magmas. Data sources; Hergt *et al.* (1989), Brewer *et al.* (1992), Elliot *et al.* (1995), Fleming *et al.* (1995), Molzahn *et al.* (1996), Wilhelm & Worner (1996), Antonini *et al.* (1999), Elliot *et al.* (1999), Elliot & Fleming (2004), Riley *et al.* (2006). Falkland Islands samples symbols as for Fig. 4.

Fig. 12.  $\epsilon\text{Nd}_{182}$  versus  $^{87}\text{Sr}/^{86}\text{Sr}_{182}$  for Falkland Islands PST intrusions (filled dots) Karoo low TiO<sub>2</sub> volcanic rocks (open circles), Dronning Maud Land CT1 (open triangles), CT2 (filled diamonds) and CT3 (filled triangles) basalts. Details of the parameters used in generating the three AFC mixing lines (CT1, PST-1 and PST-2) are given in Table 4. Each cross represents 1% AFC. Data sources for Karoo Province; Galerne *et al.* (2008); McClintock *et al.* (2008); Neumann *et al.* (2011).

Figure 13. a) CaO versus MgO (weight %) for Falkland Islands intrusions (black dots PST; grey dots, DIT; grey squares MAT; triangles, E-W) and Dronning Maud Land high MgO, silica-

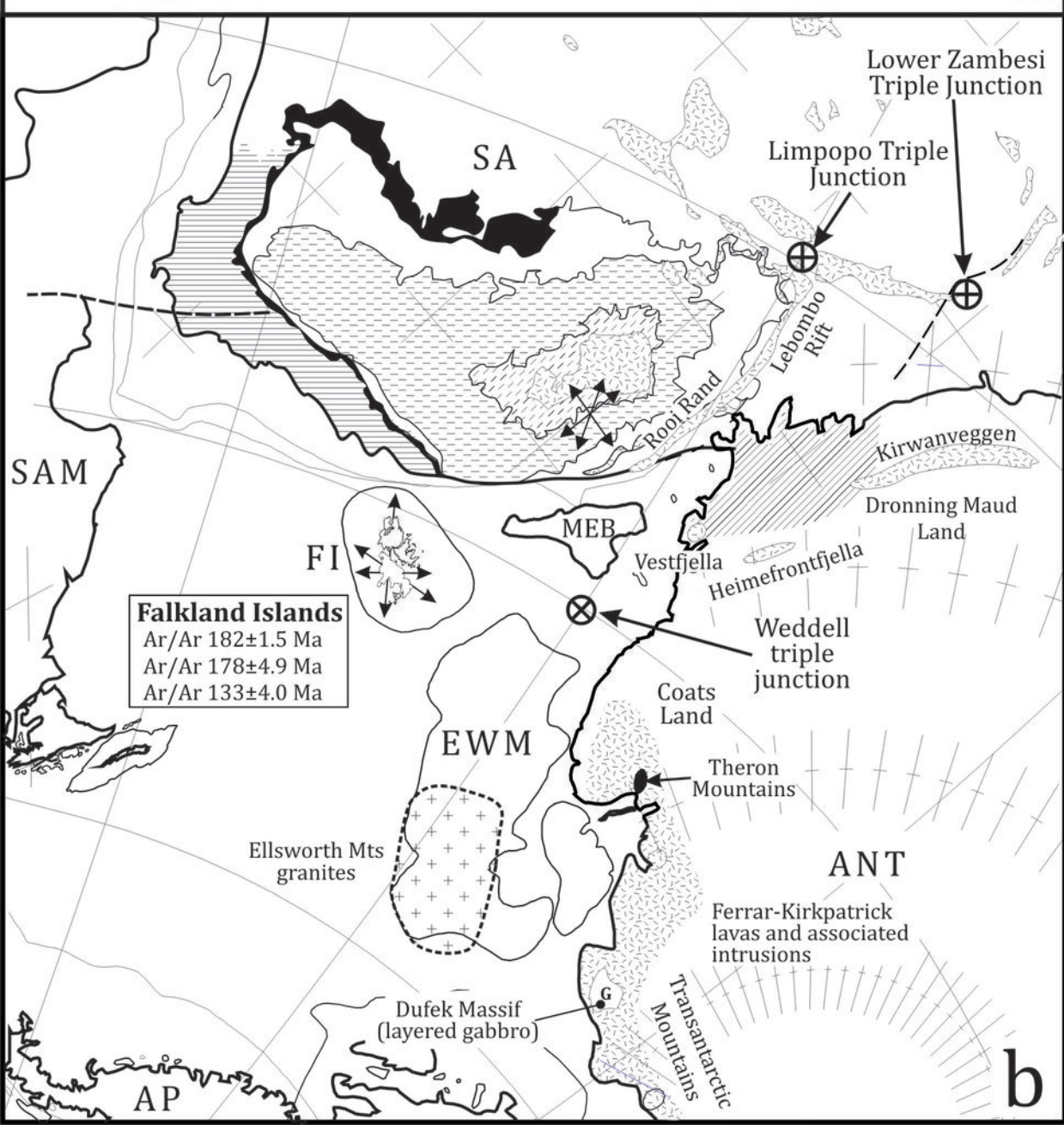
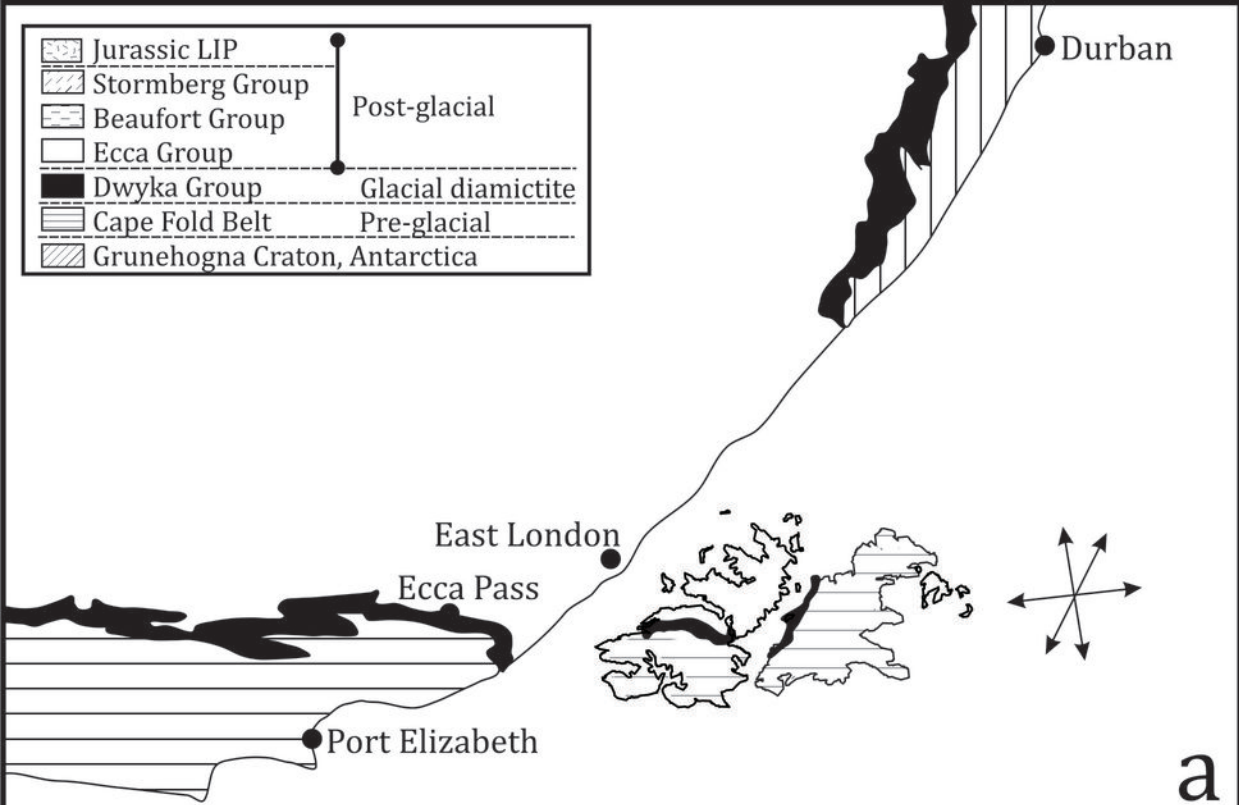


oversaturated CT1 basalts (circles). The dividing line between melts derived from peridotite and pyroxenite sources is taken from Herzberg & Asimow (2008). Lines with crosses and arrows represent the effect of accumulation of the phase indicated on the composition of PST basalt NEF9, with each cross representing 5% accumulation. b) Cr (ppm) *versus* SiO<sub>2</sub> for Falkland Islands intrusions (symbols as for Fig. 4) and high-Mg andesites from Mt Shasta (crosses; Baker *et al.* 1994).

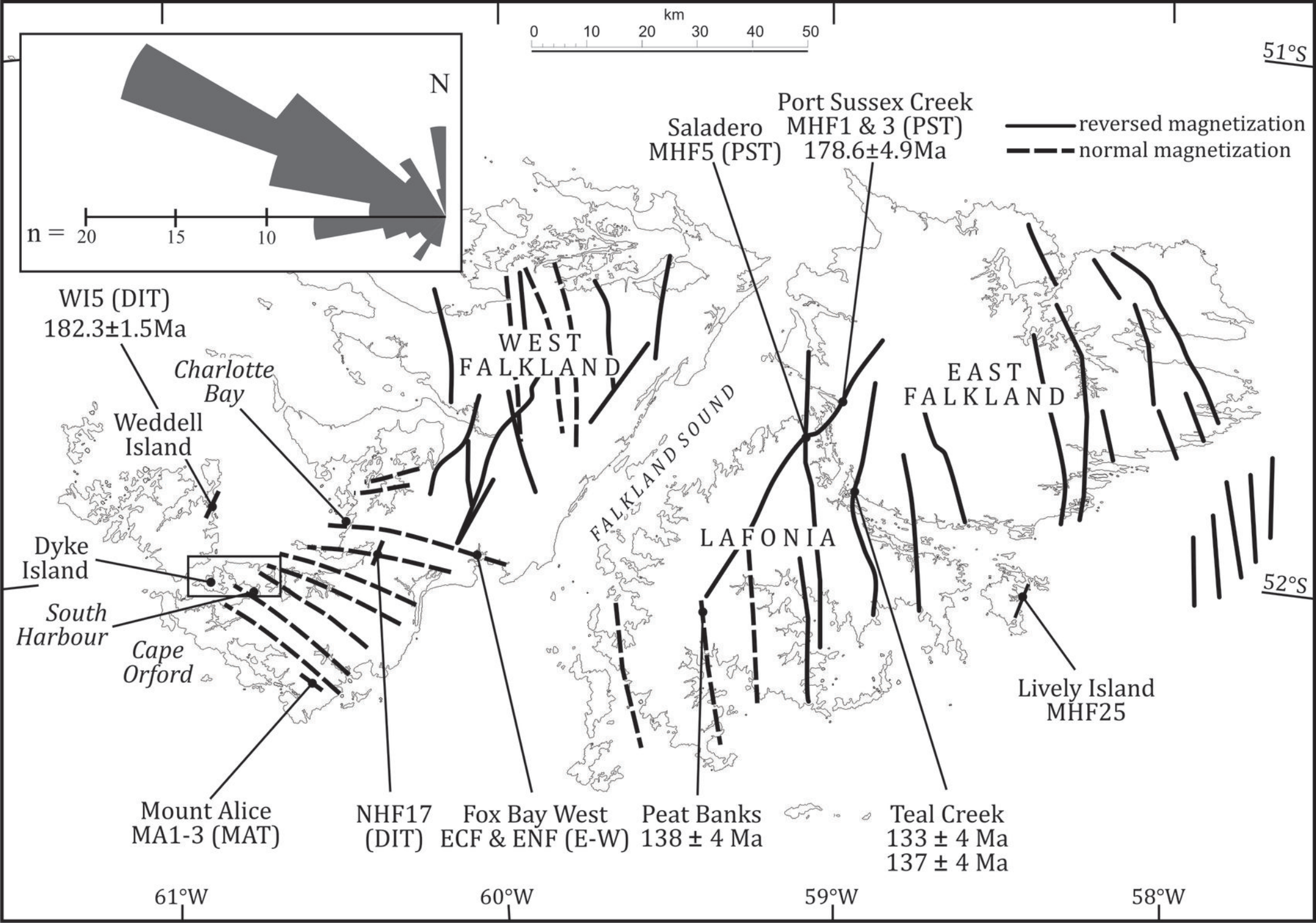
Figure 14. Ti/Zr *versus* SiO<sub>2</sub>, for a) Karoo LIP volcanic rocks and b) Ferrar LIP volcanic rocks. Note that the KwaZulu-Natal and Theron Mountains low TiO<sub>2</sub> samples are considered to be magma types transitional between Karoo and Ferrar types. Data sources; Transantarctic Mountains and Theron Mountains; Hergt *et al.* (1989), Brewer *et al.* (1992), Elliot *et al.* (1995), Fleming *et al.* (1995), Molzahn *et al.* (1996), Wilhelm & Worner (1996), Antonini *et al.* (1999), Elliot *et al.* (1999), Elliot & Fleming (2004). Karoo (including Dronning Maud Land) Luttinen *et al.* (1998), Luttinen & Furnes (2000), Heinonen & Luttinen (2008), Heinonen *et al.* (2010; 2013; 2014) Neumann *et al.* (2011). Kirwanveggan; Harris *et al.* (1990).

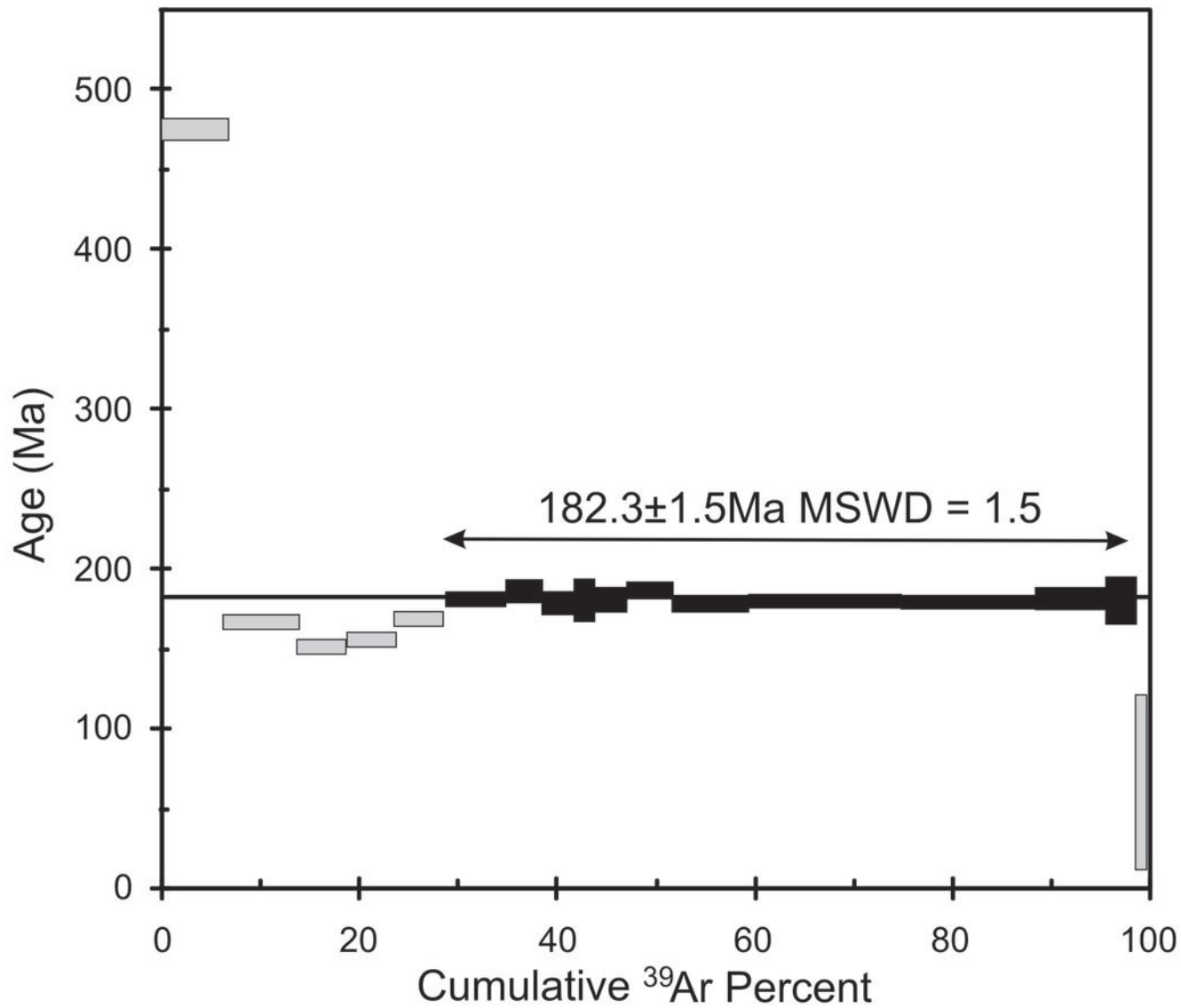
Figure 15. a) Olivine equilibration temperatures (°C) *versus* Mg# of liquid in equilibrium with olivine for Ahlmannryggen dykes (filled dots; Heinonen & Luttinen 2008), Vestfjella high TiO<sub>2</sub> ferropicrite (filled triangles; Heinonen *et al.* 2013), Etendeka picrite (open squares; Kieding *et al.* 2011) and Falklands Islands MAT intrusion (star in circle) and E-W intrusions (open triangles). Olivine equilibration temperatures have been calculated according to the scheme of Putirka *et al.* (2007). Vertical lines connecting points for Ahlmannryggen samples are calculated equilibration temperatures for different olivine phenocrysts in individual whole-rock samples. Figures in italics are T<sub>P</sub> from melt inclusions for Etendeka samples plotted in Fig. 15a (Kieding *et al.* 2011). b) Inferred temperature-pressure conditions at which fractional melting terminated for calculated primary magmas from Dronning Maud Land, the Karoo Province of southern Africa, Ferrar dolerites of Antarctica and picrites of the Etendeka Province of western Africa. The diagram was constructed following the methods of Herzberg and Gazel (2009) with data for the Ferrar province and Iceland from Hole (2015). Samples with MgO > 20 weight % are shown schematically following an adiabatic pathway for T<sub>P</sub> = 1640°C. The diagonally shaded box on the temperature axis is the range of olivine equilibration temperatures, calculated at 0 GPa, for olivine in ferro-picrite dykes from Dronning Maud following the method of Putirka *et al.* (2007), and the box labelled 'MAT & E-W' is the same calculations for MAT and E-W intrusions. Adiabatic melting paths are labelled with mantle potential temperature. 2σ error bars are from Hole (2015). c) T<sub>P</sub> calculated from melt inclusions in ultra-magnesian olivines from the

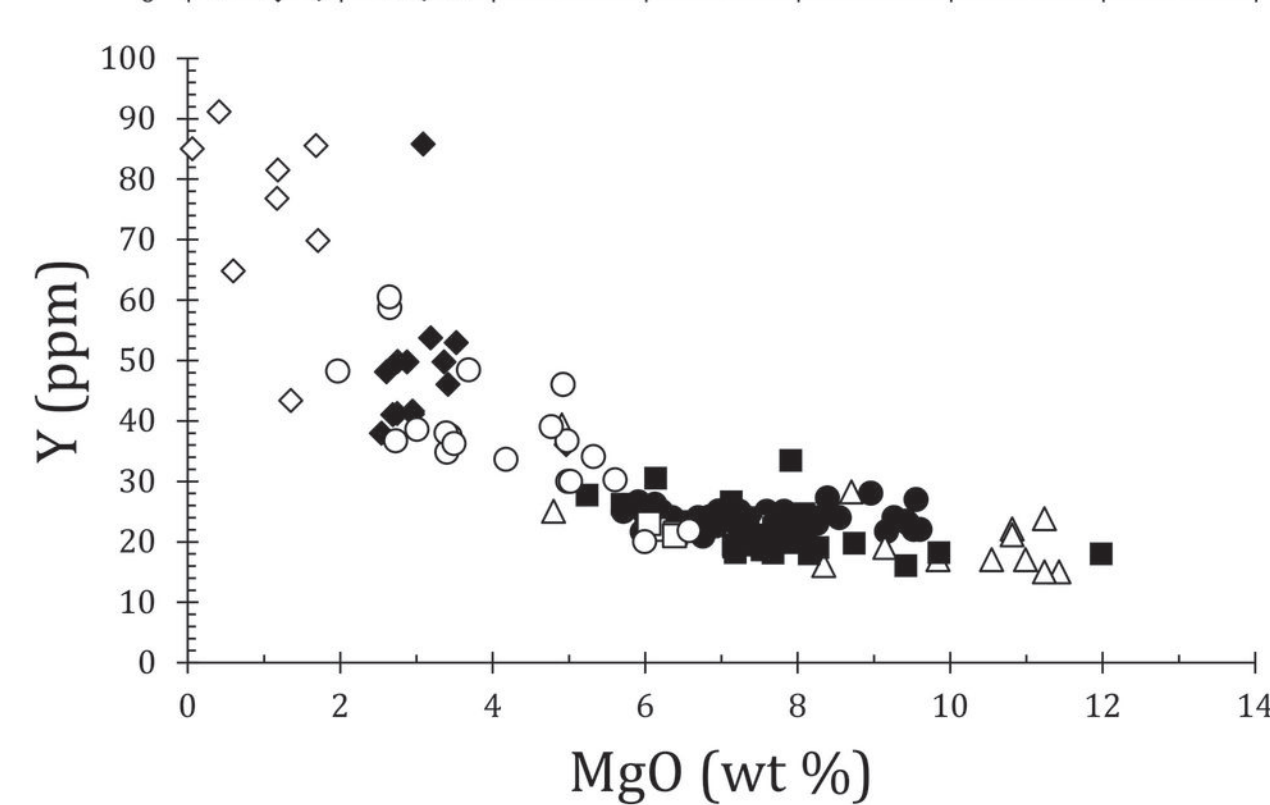
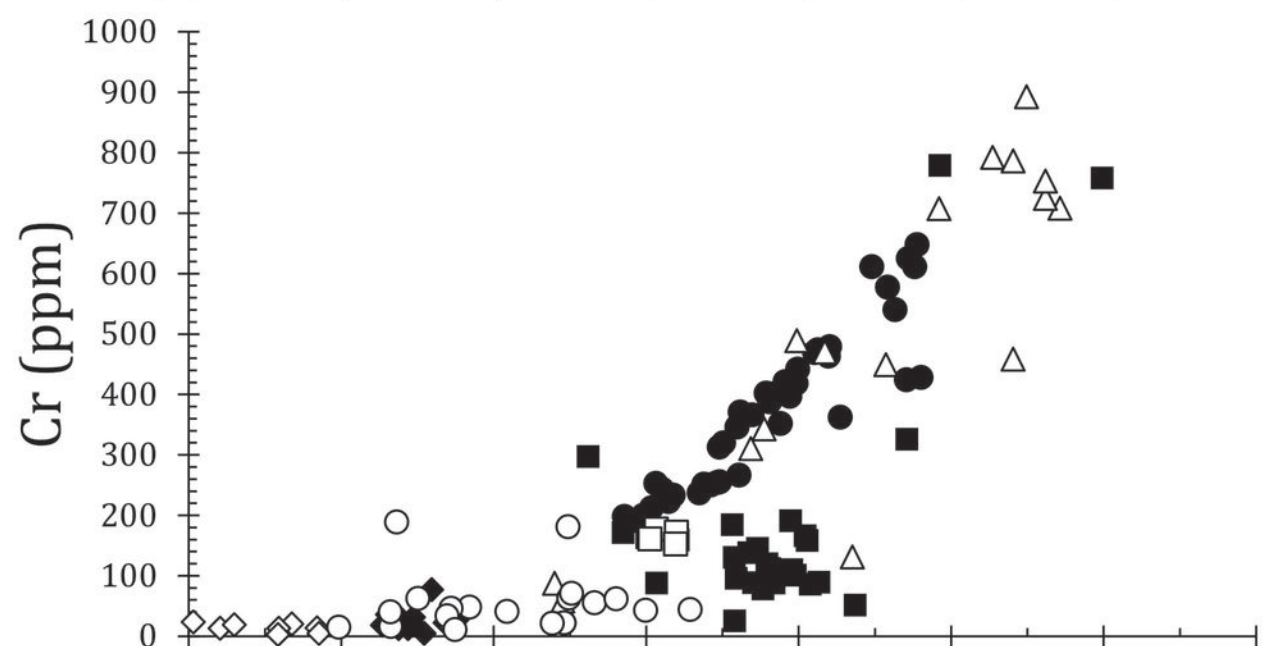
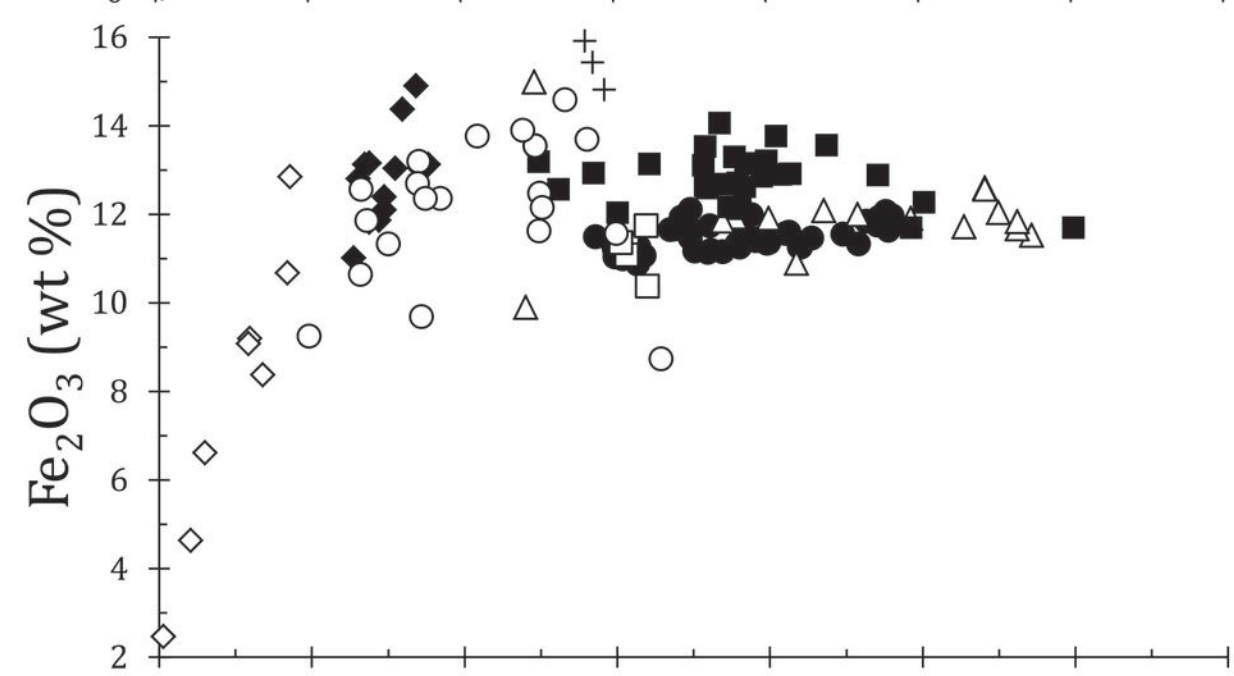
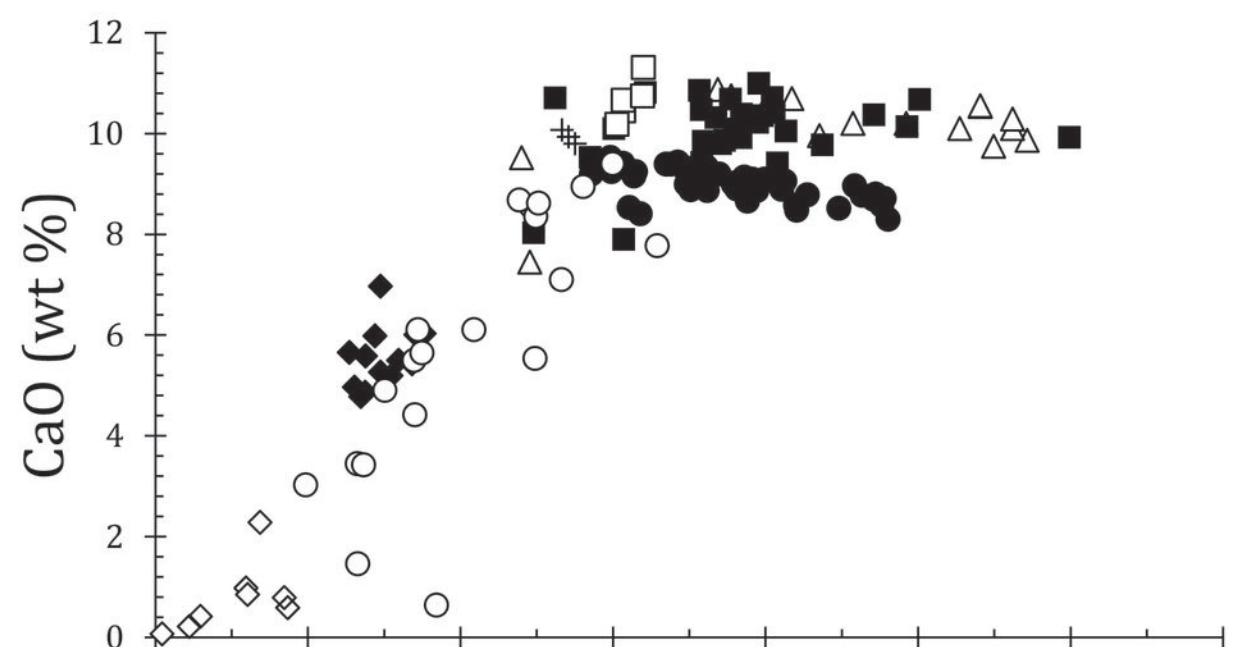
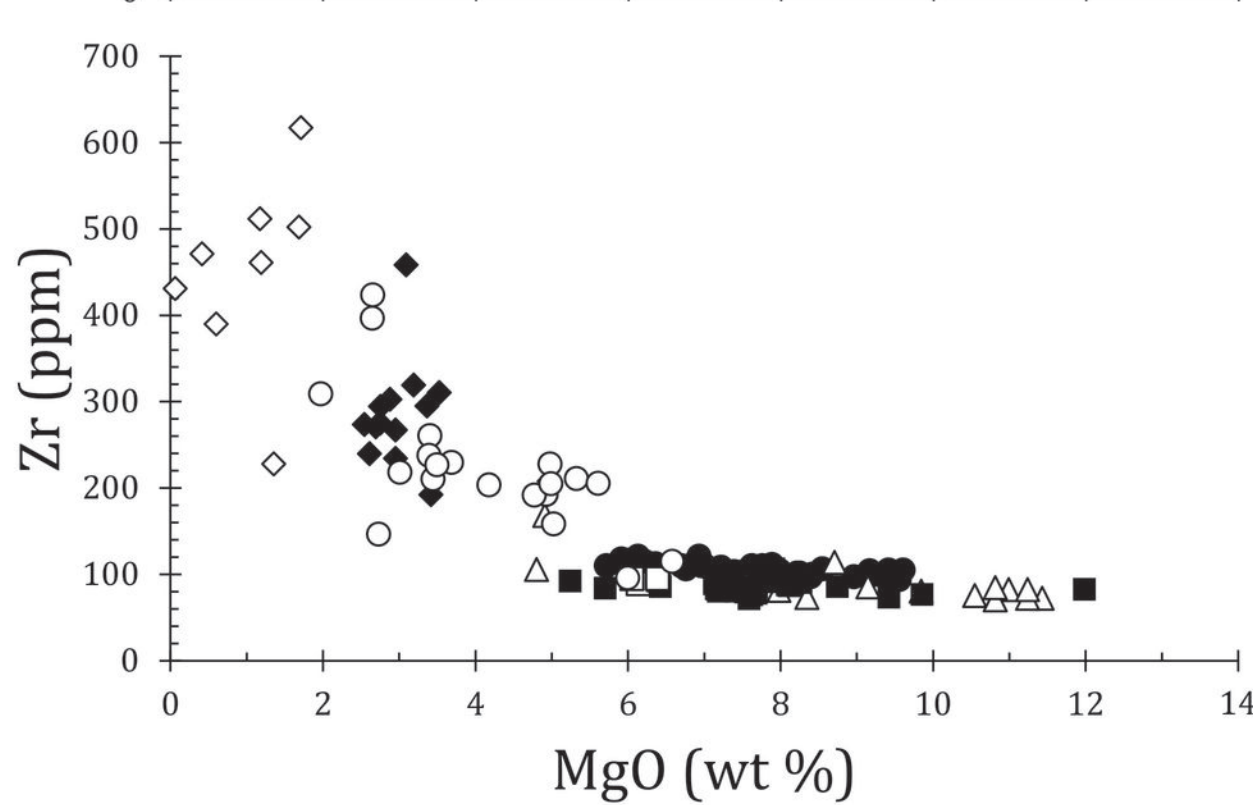
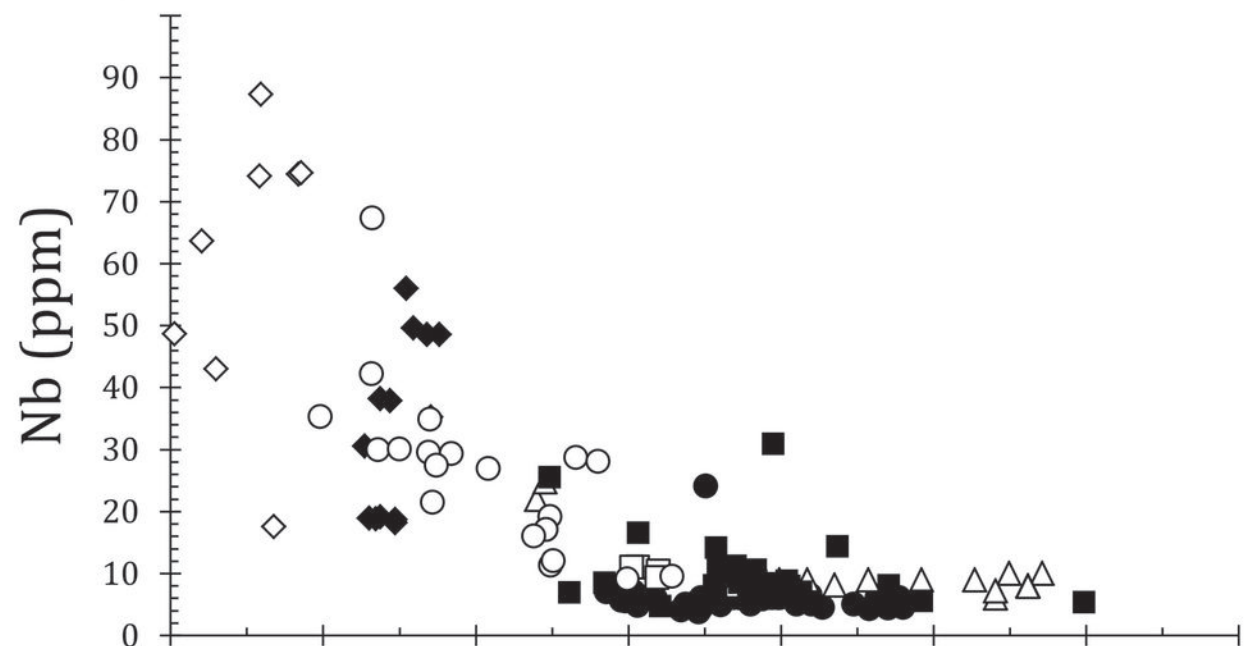
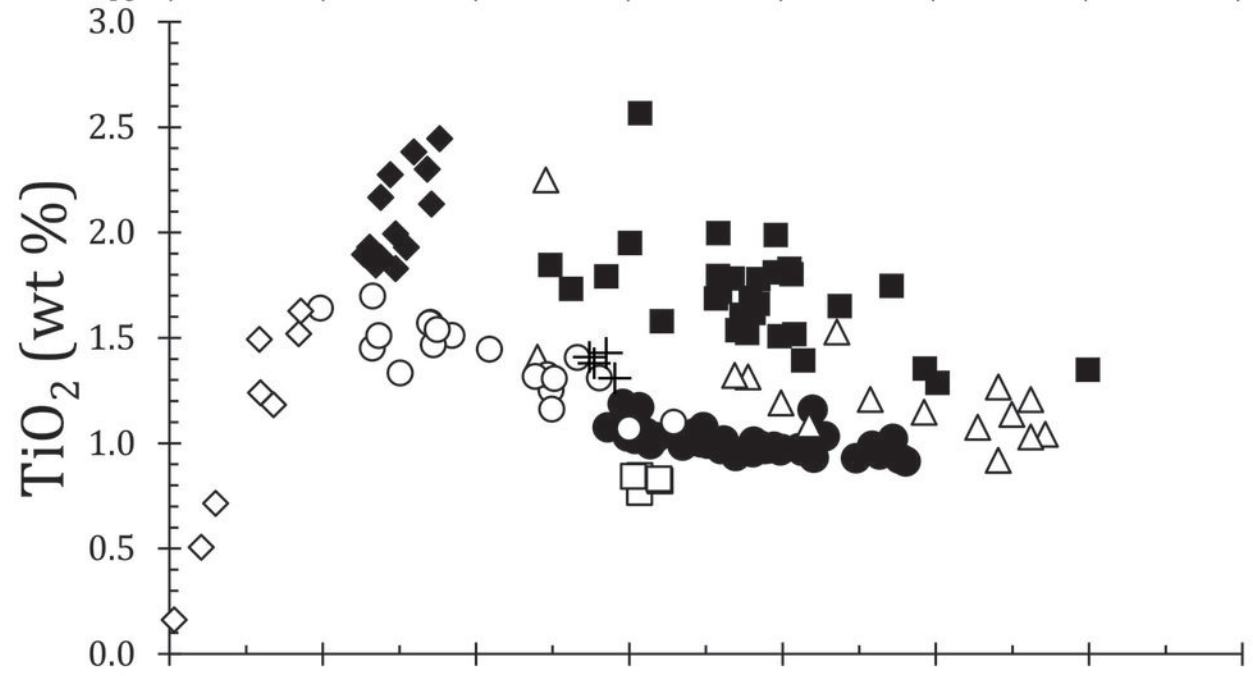
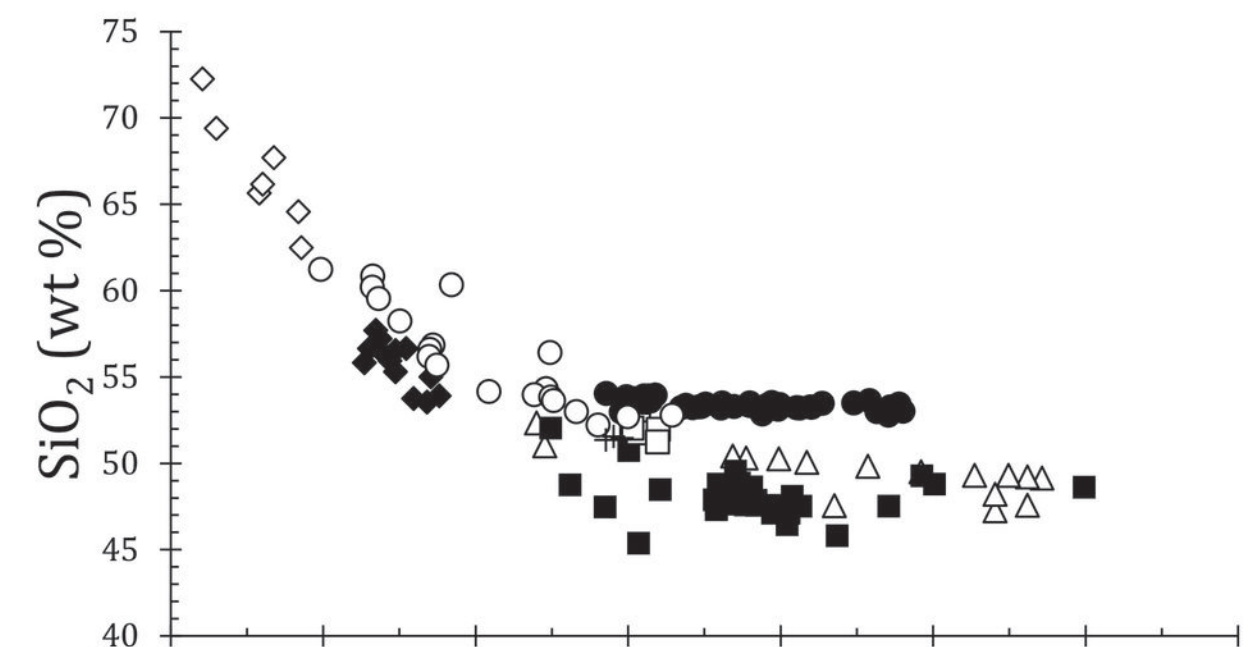
798 Etendeka Province *versus* olivine equilibration temperatures for the same samples. Data from  
799 Keiding *et al.* (2011).  
800











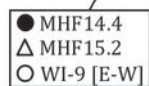


Diopside

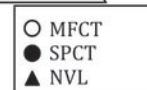
Hedenbergite

MAT &amp; EW

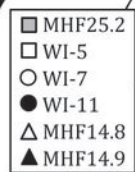
Antarctica



Mg-pigeonite



DIT

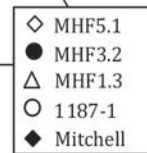


FAR1503

PST

Augite

Fe-augite

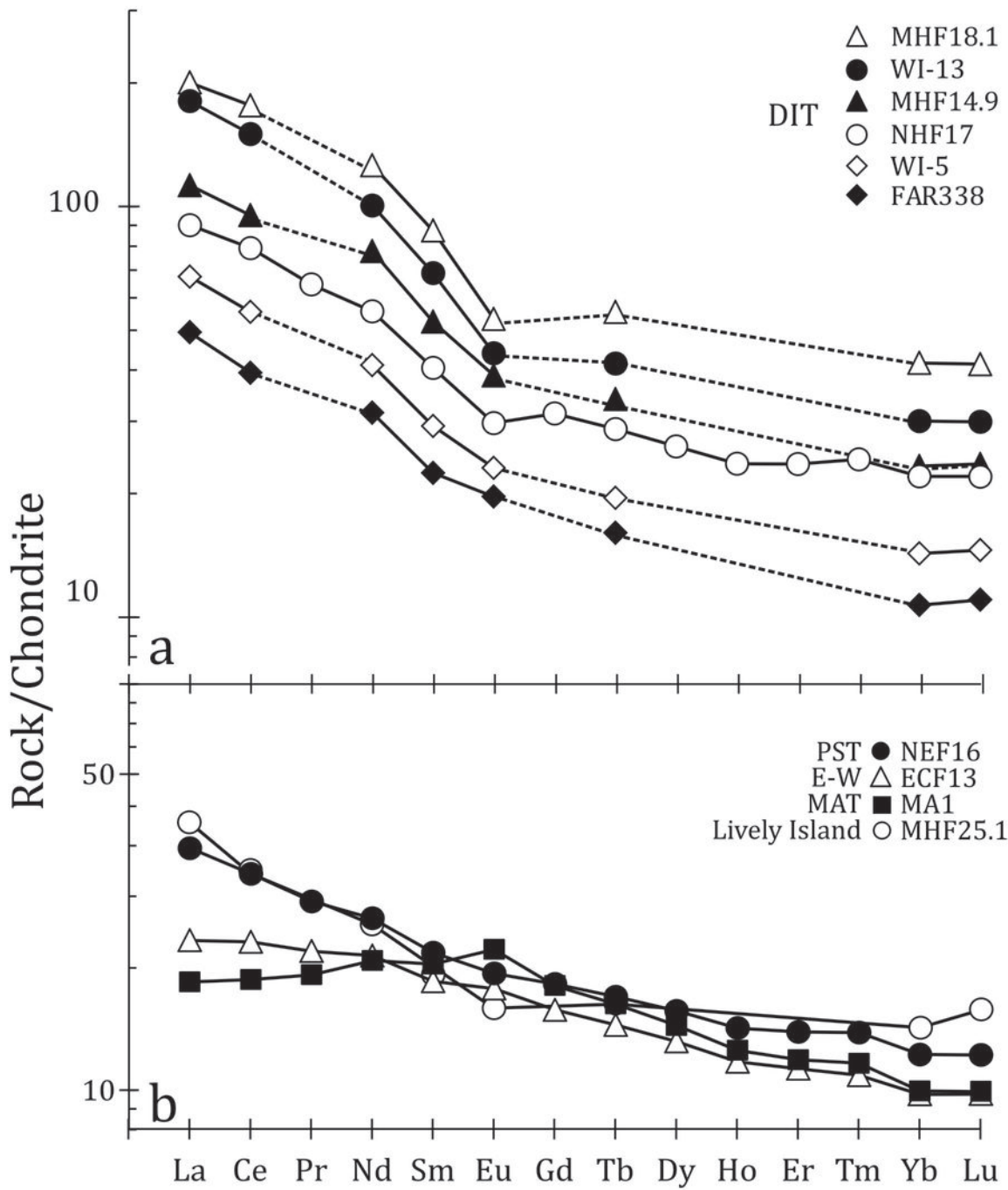


Enstatite

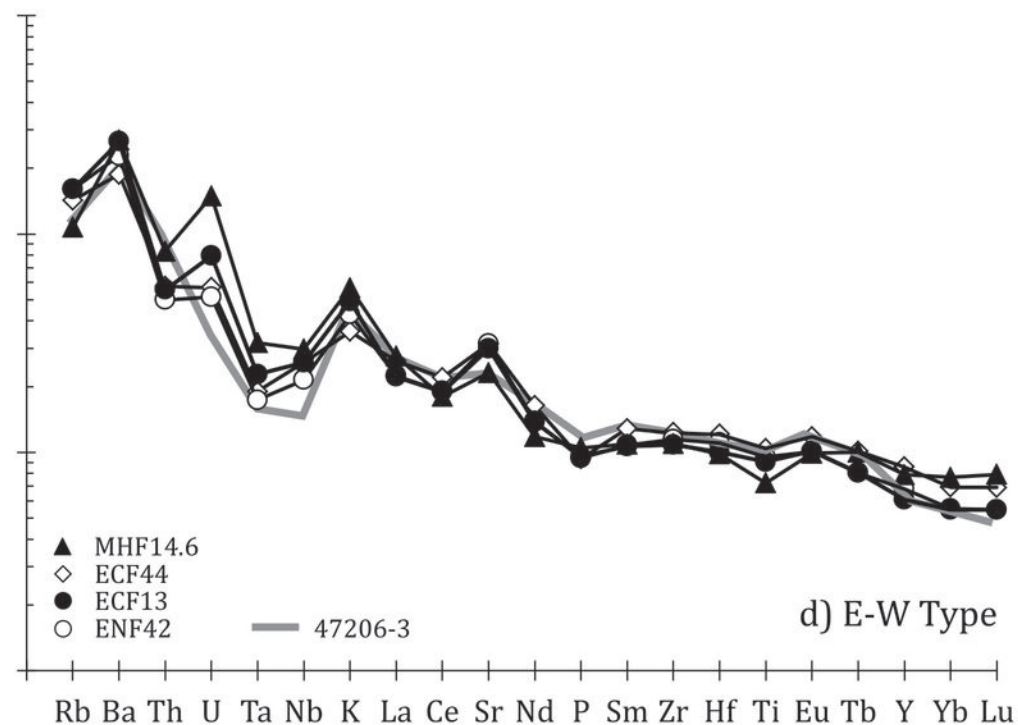
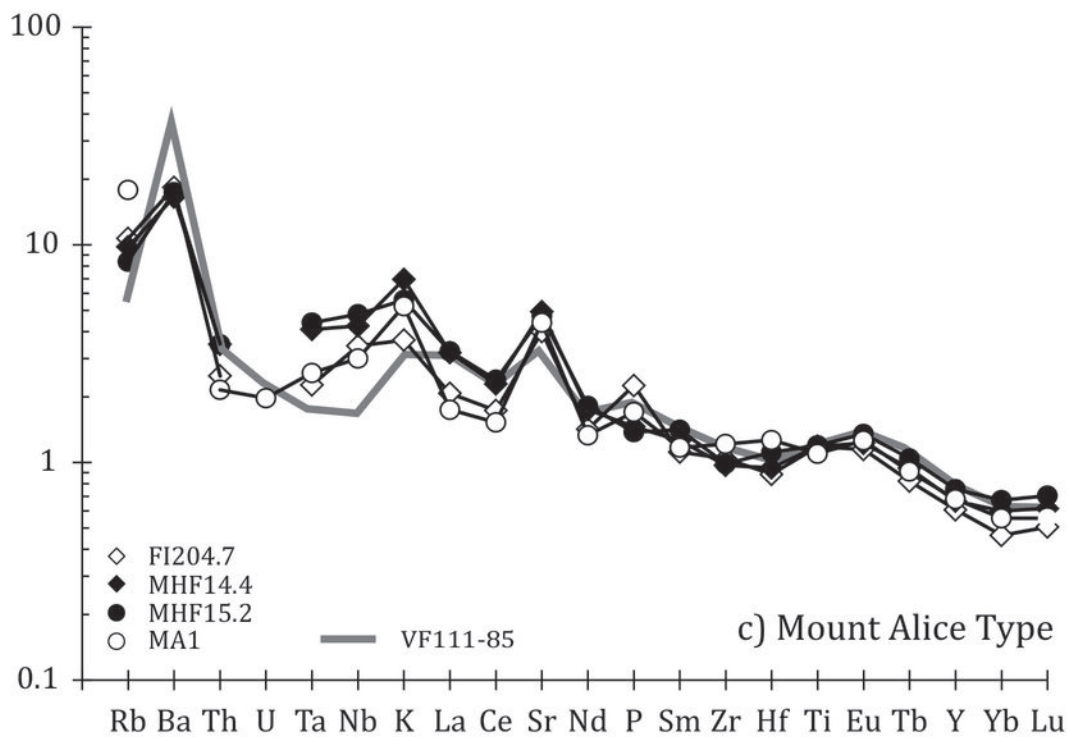
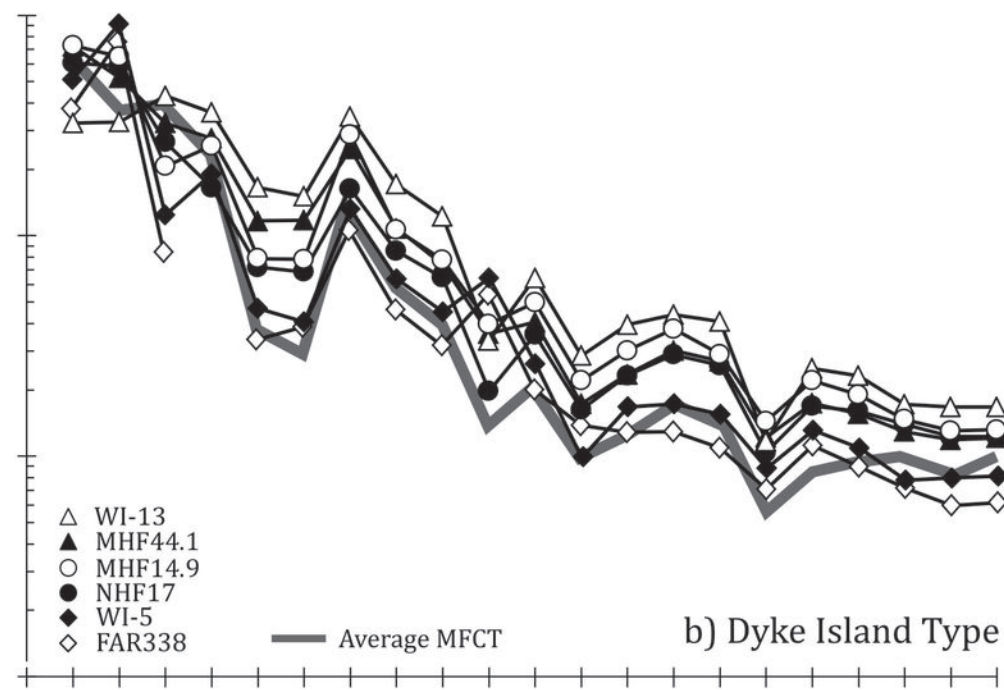
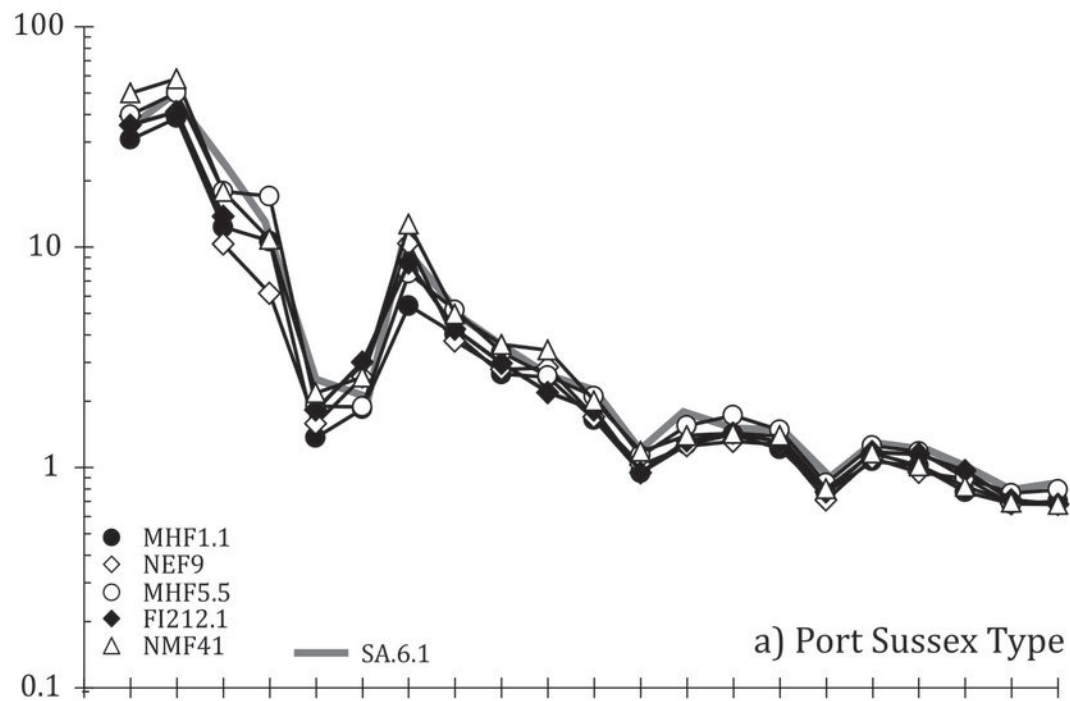
Fo<sub>70-80</sub>

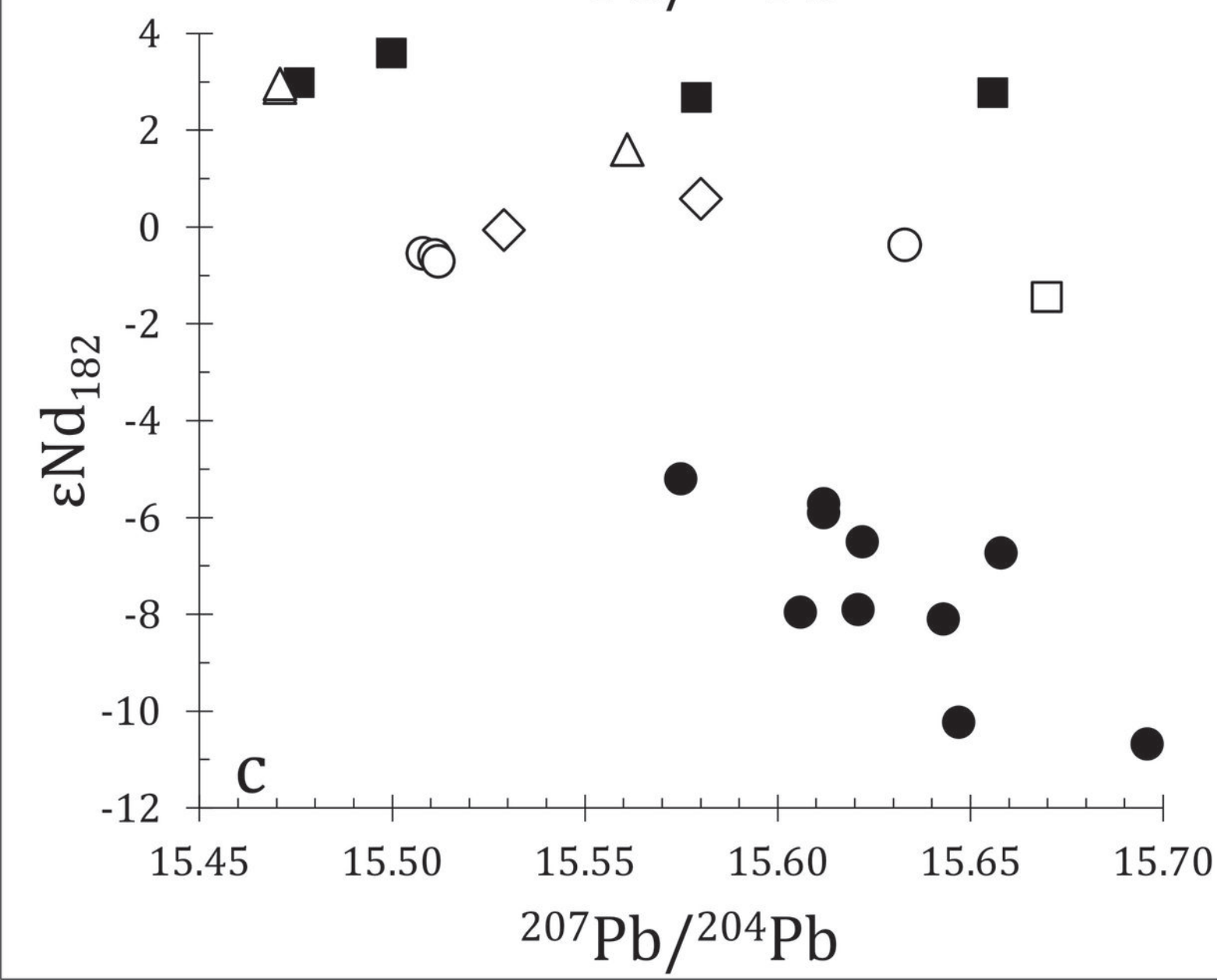
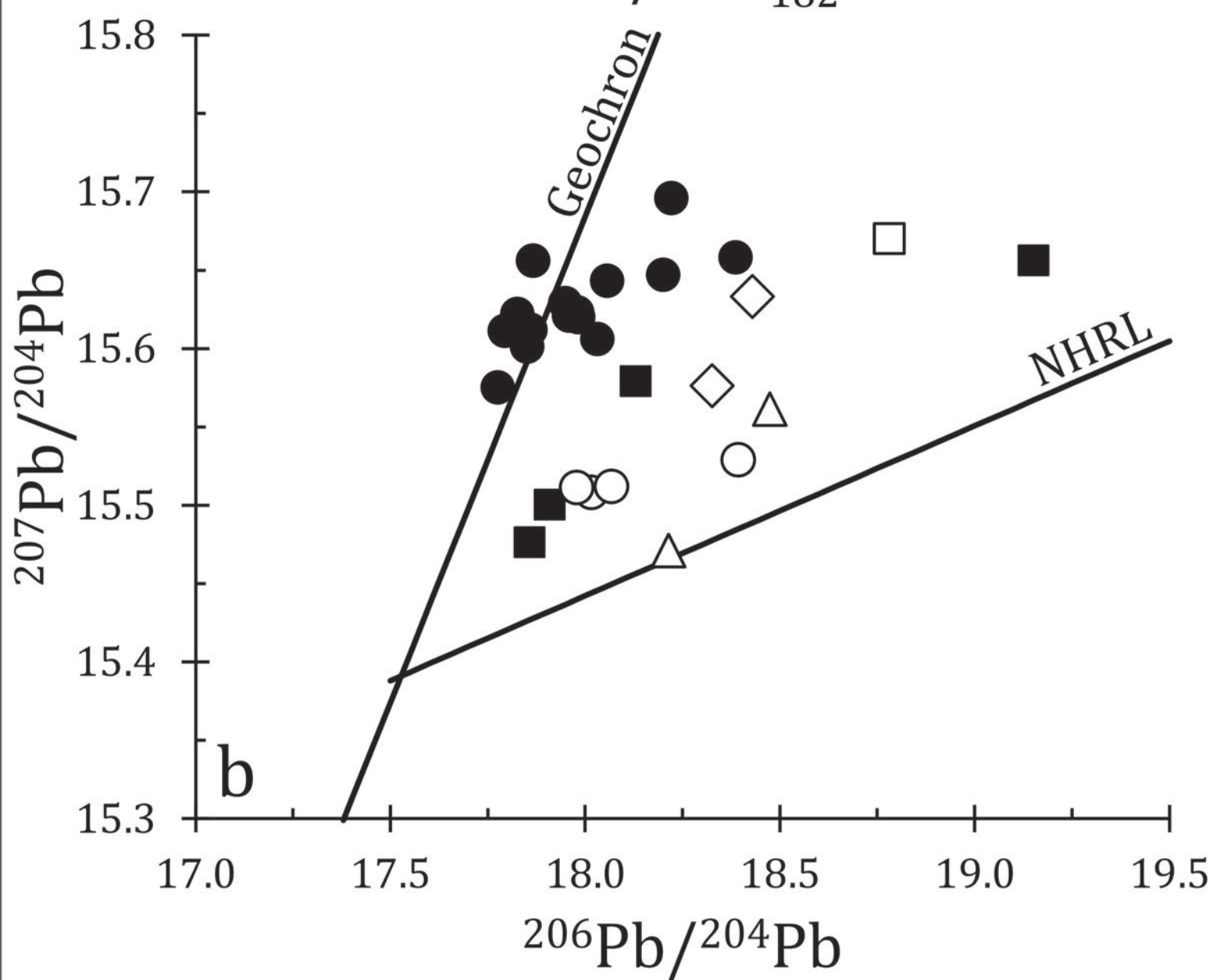
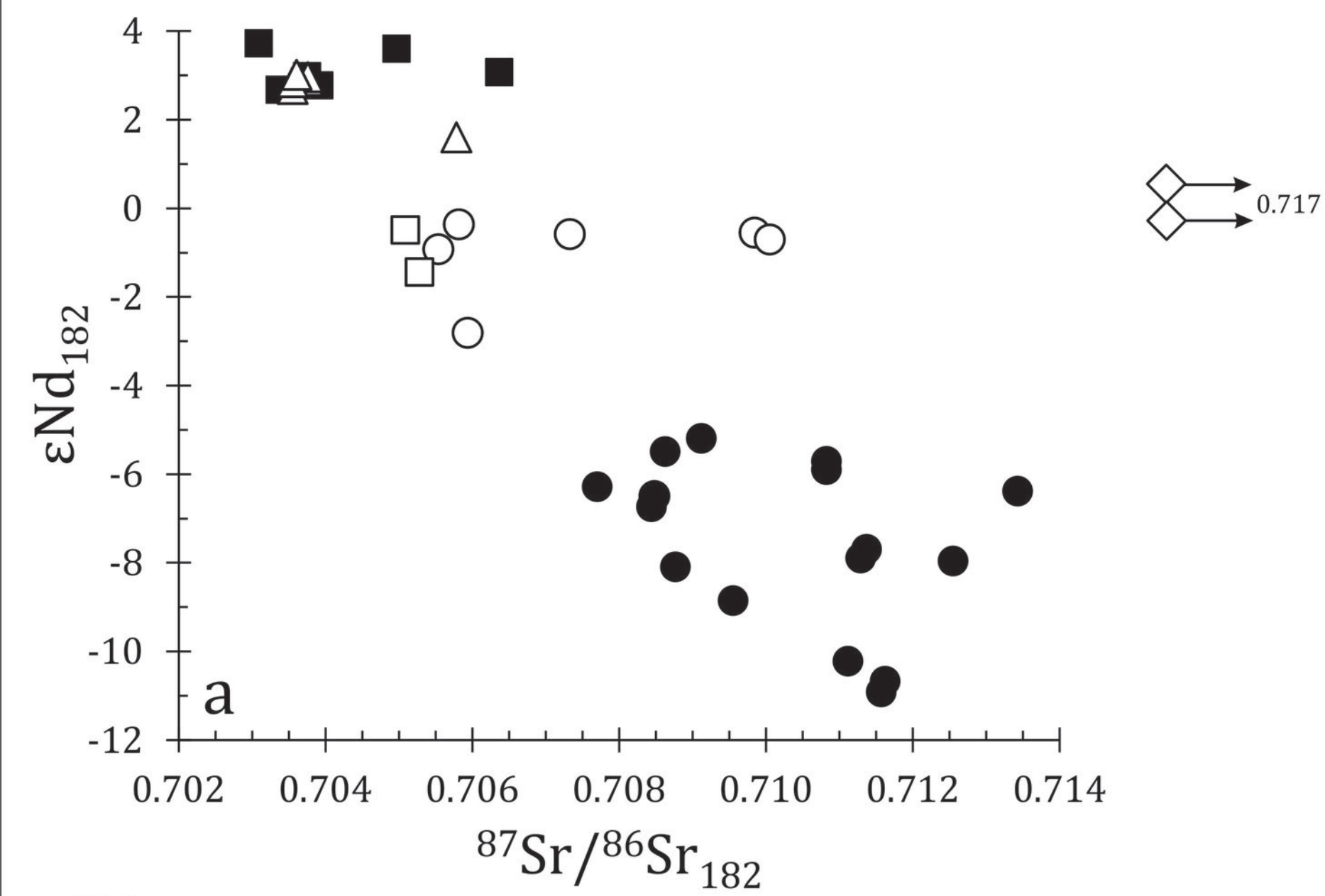
Ferrosilite

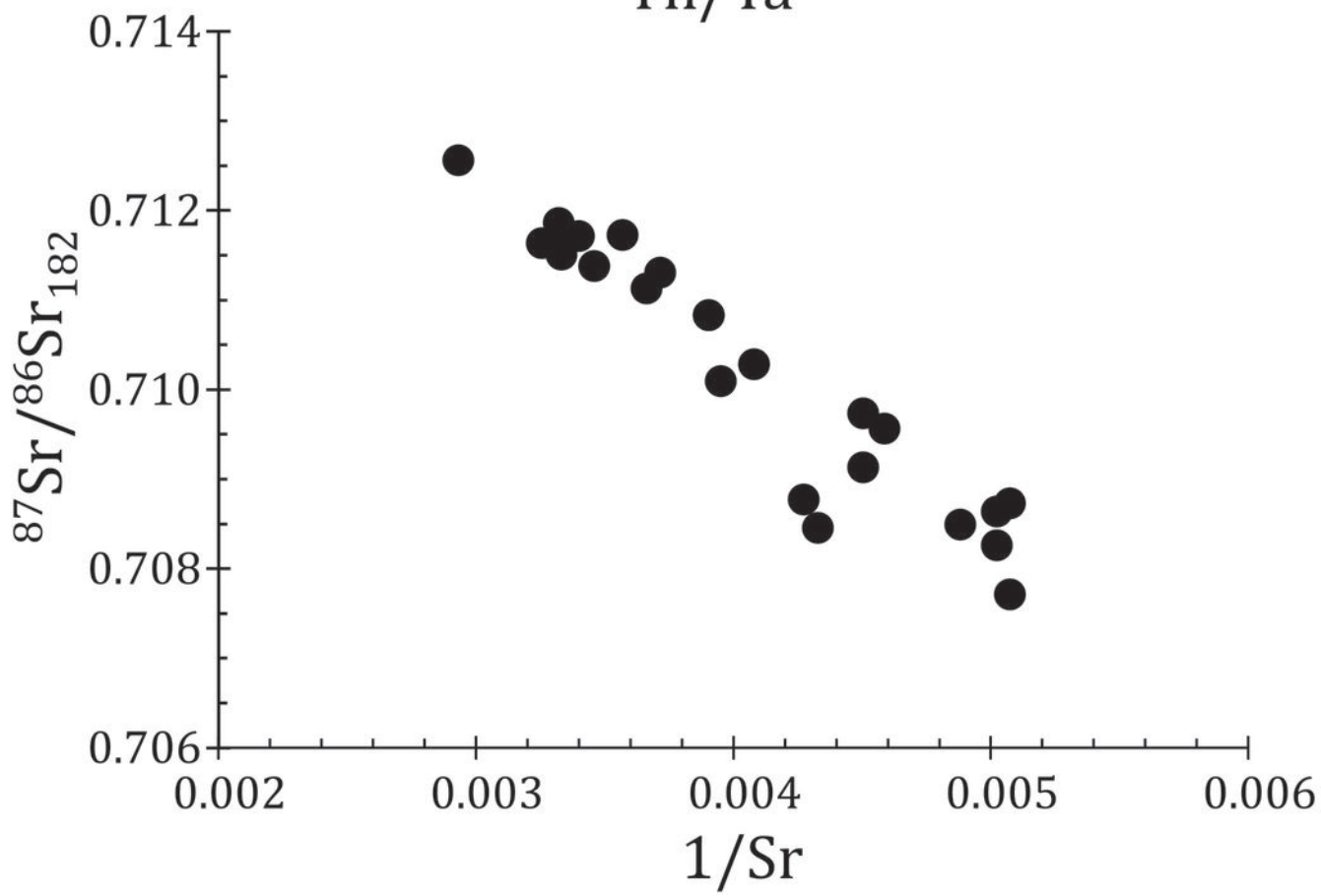
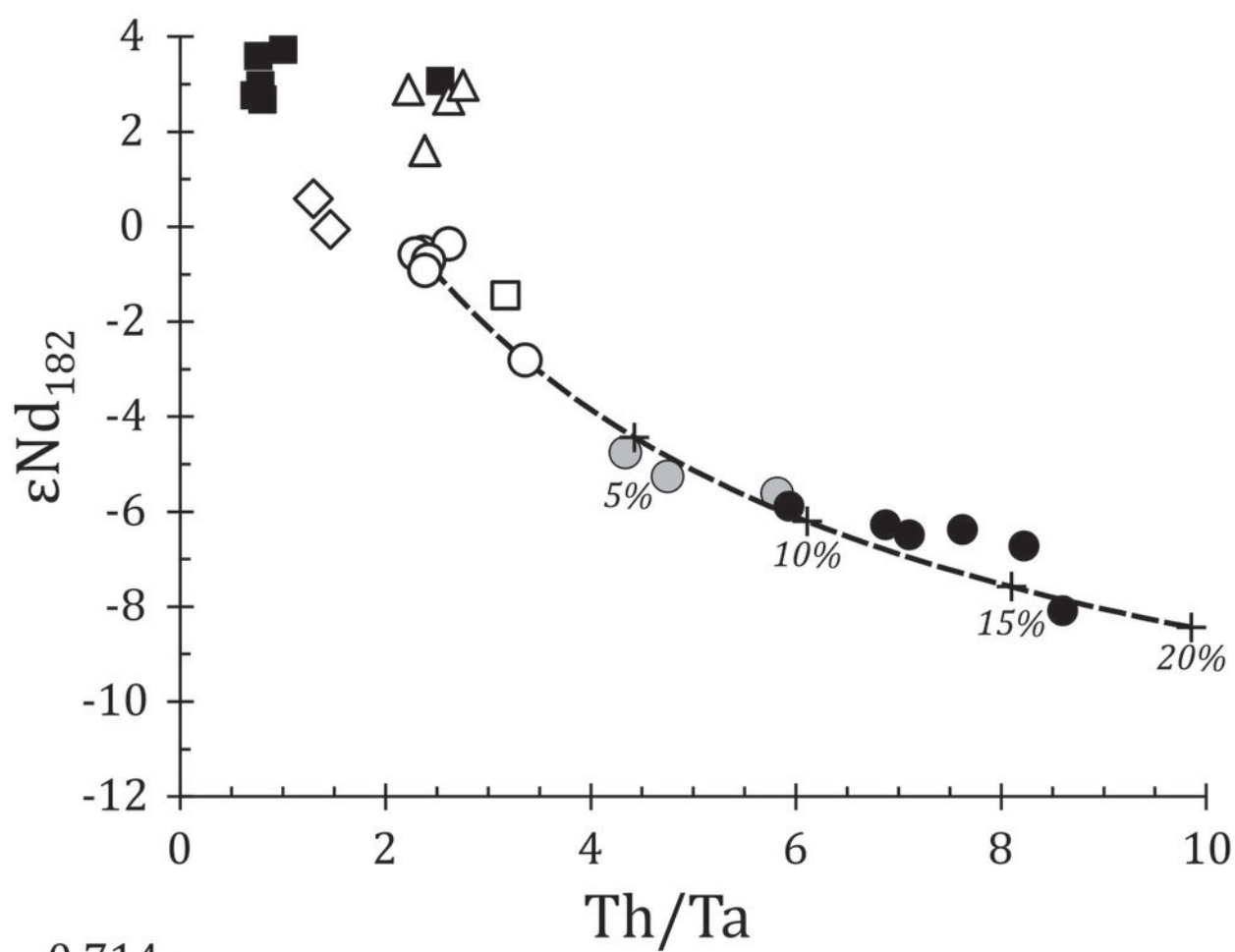
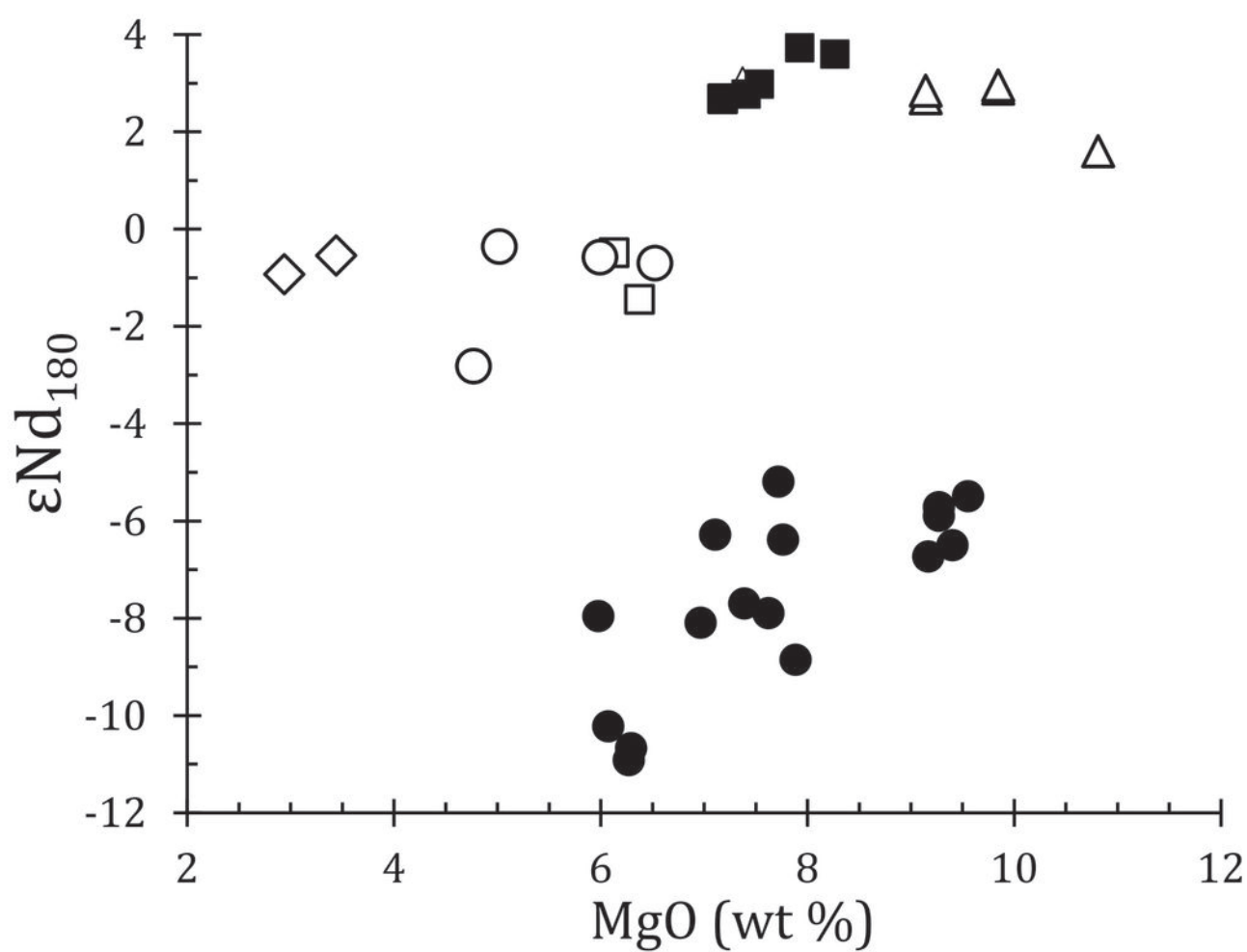


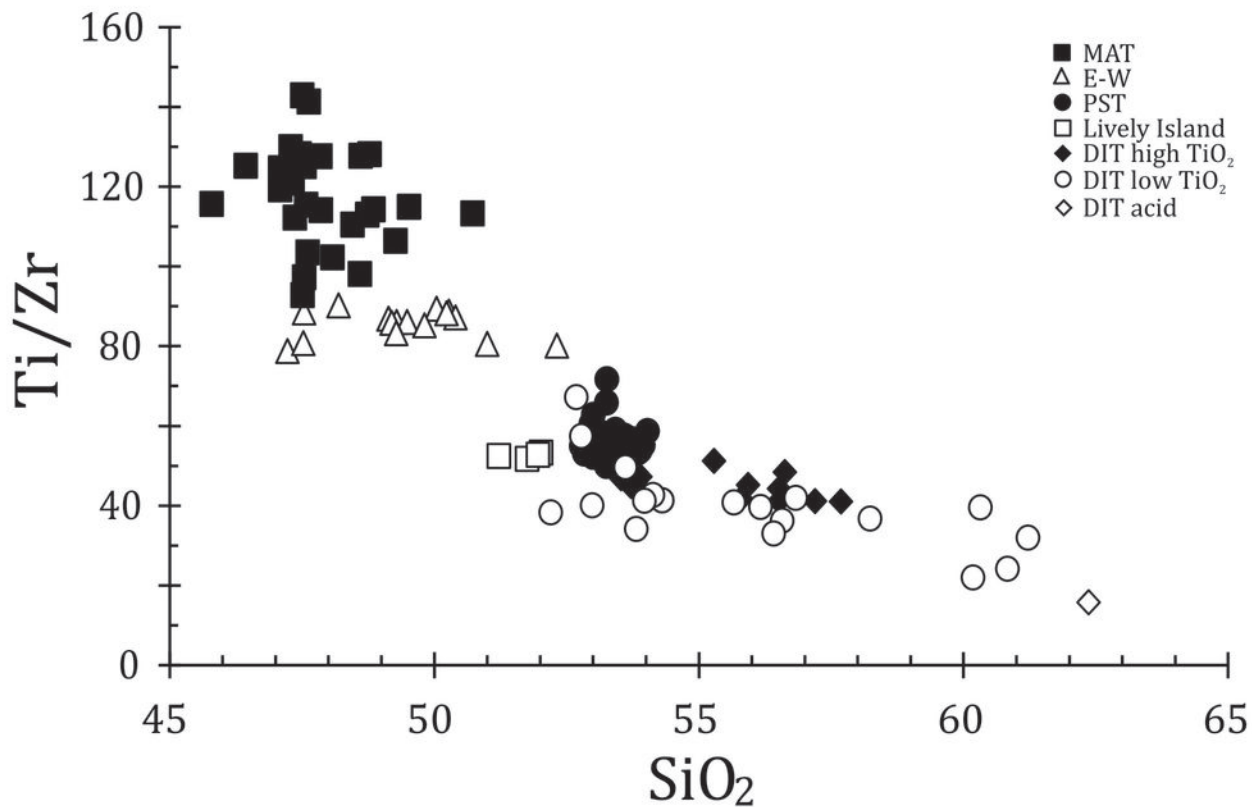


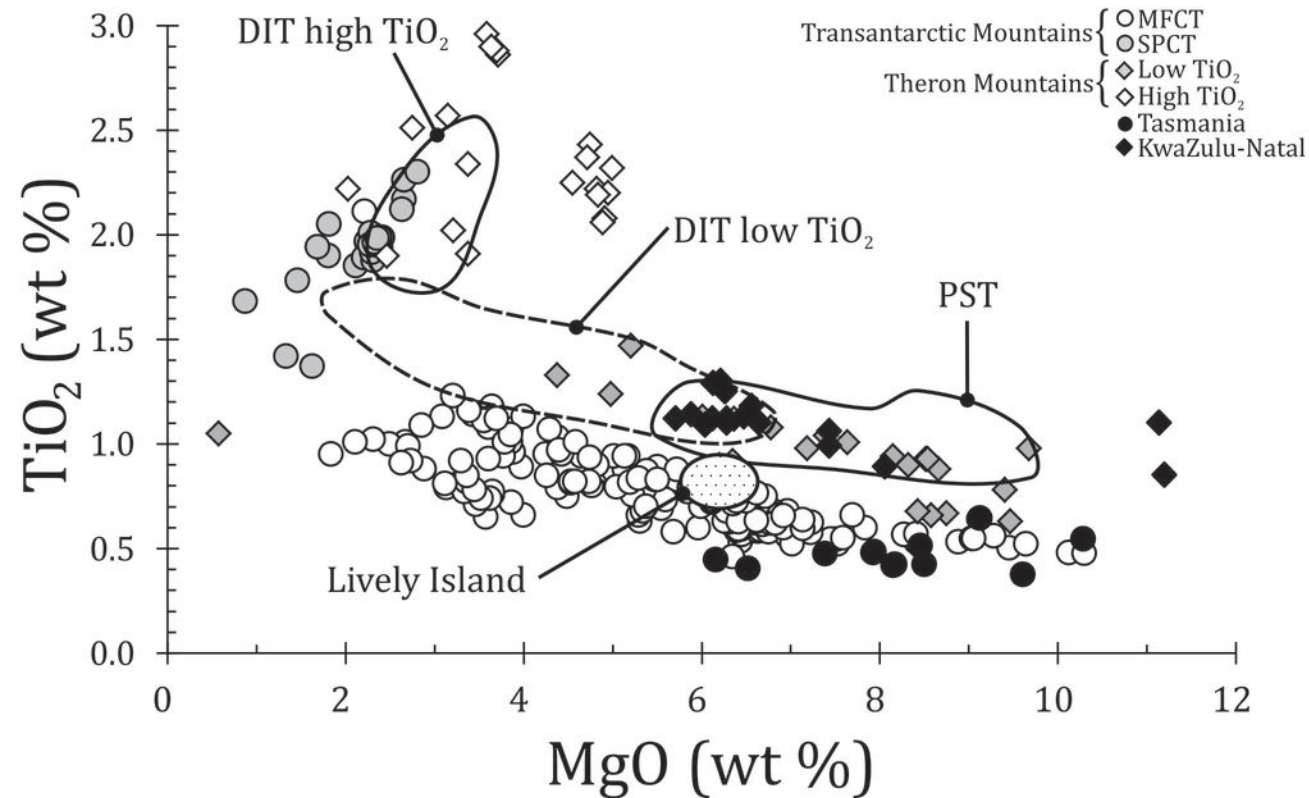
Rock/N-ORB



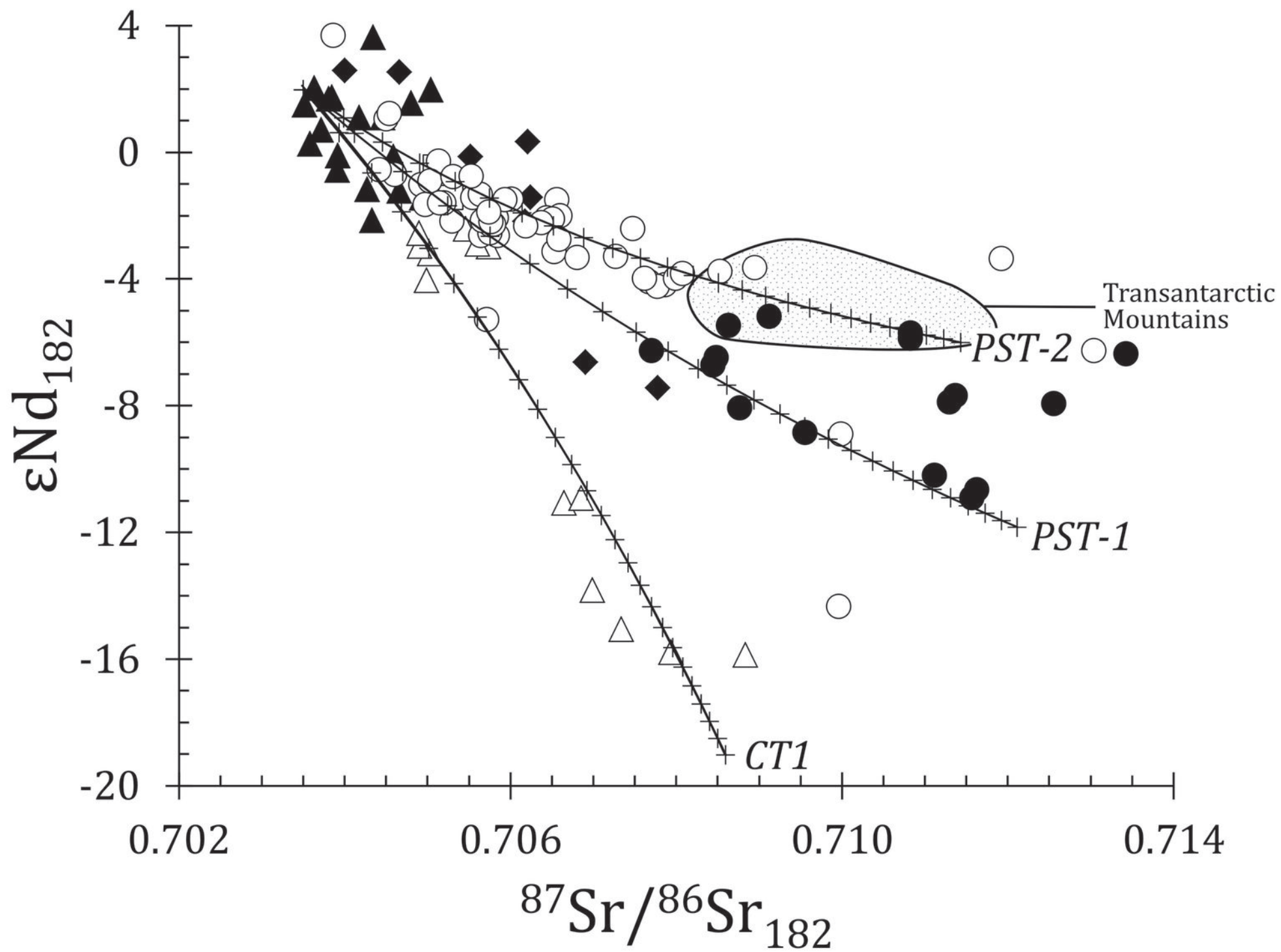




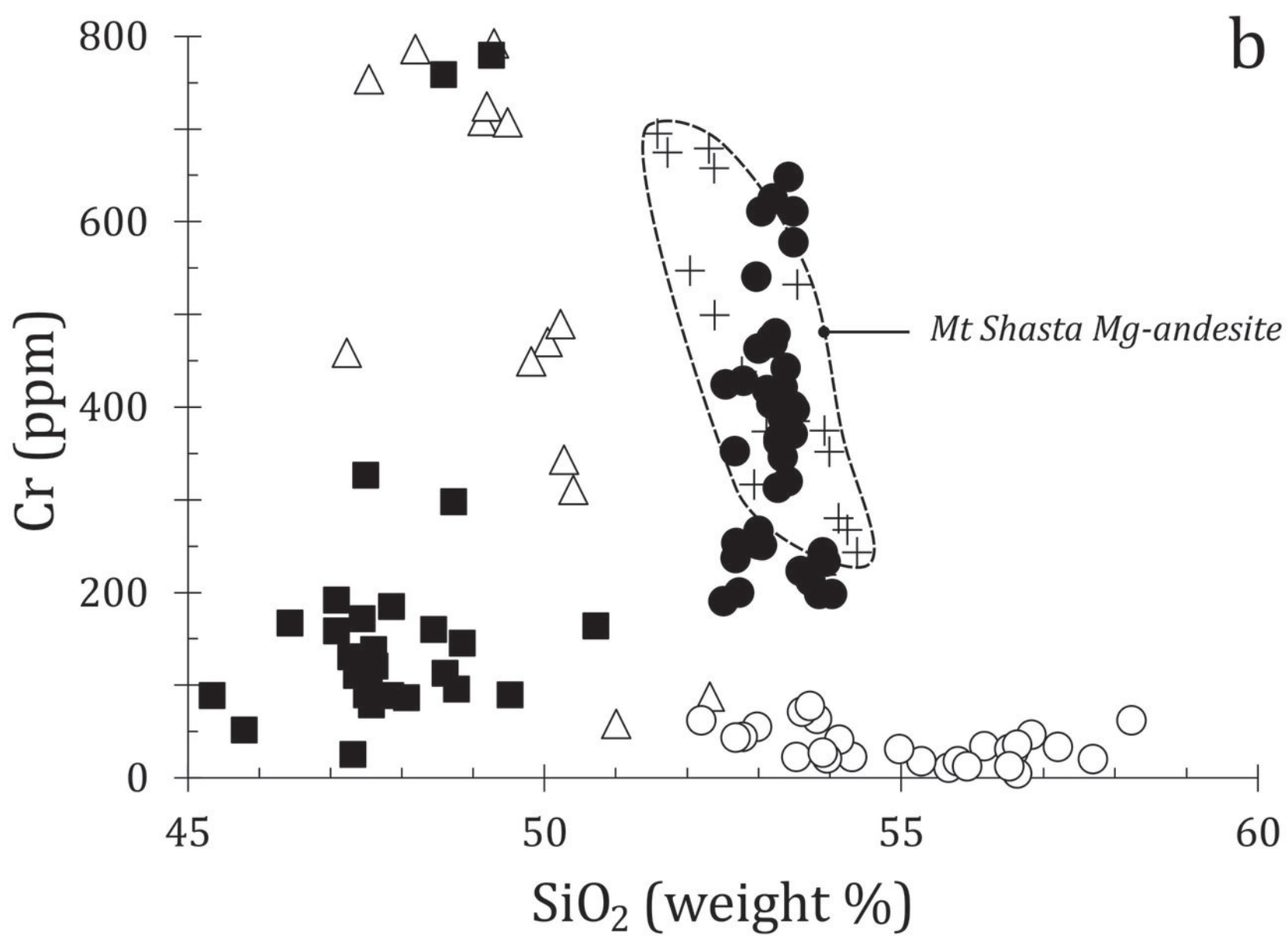
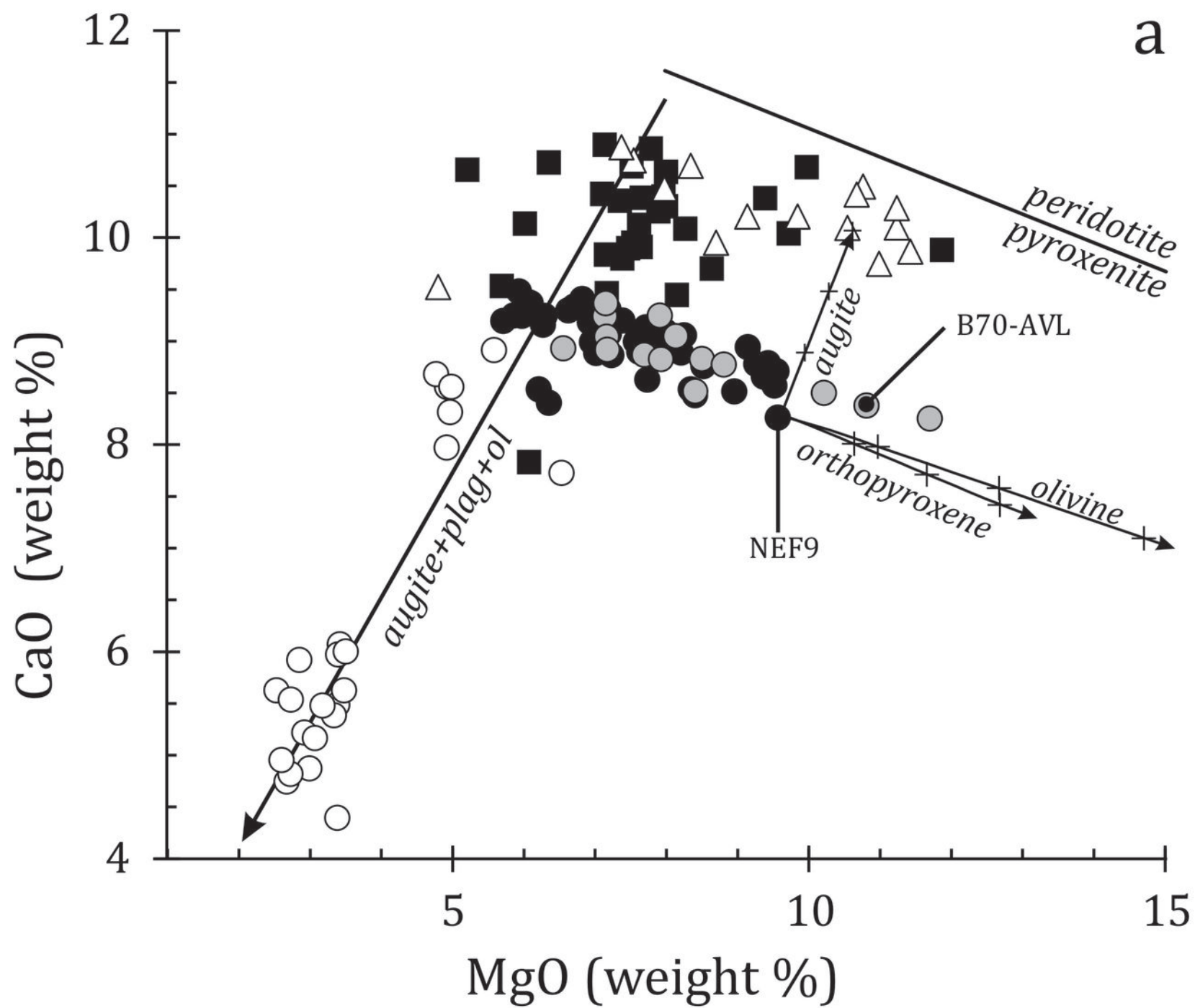


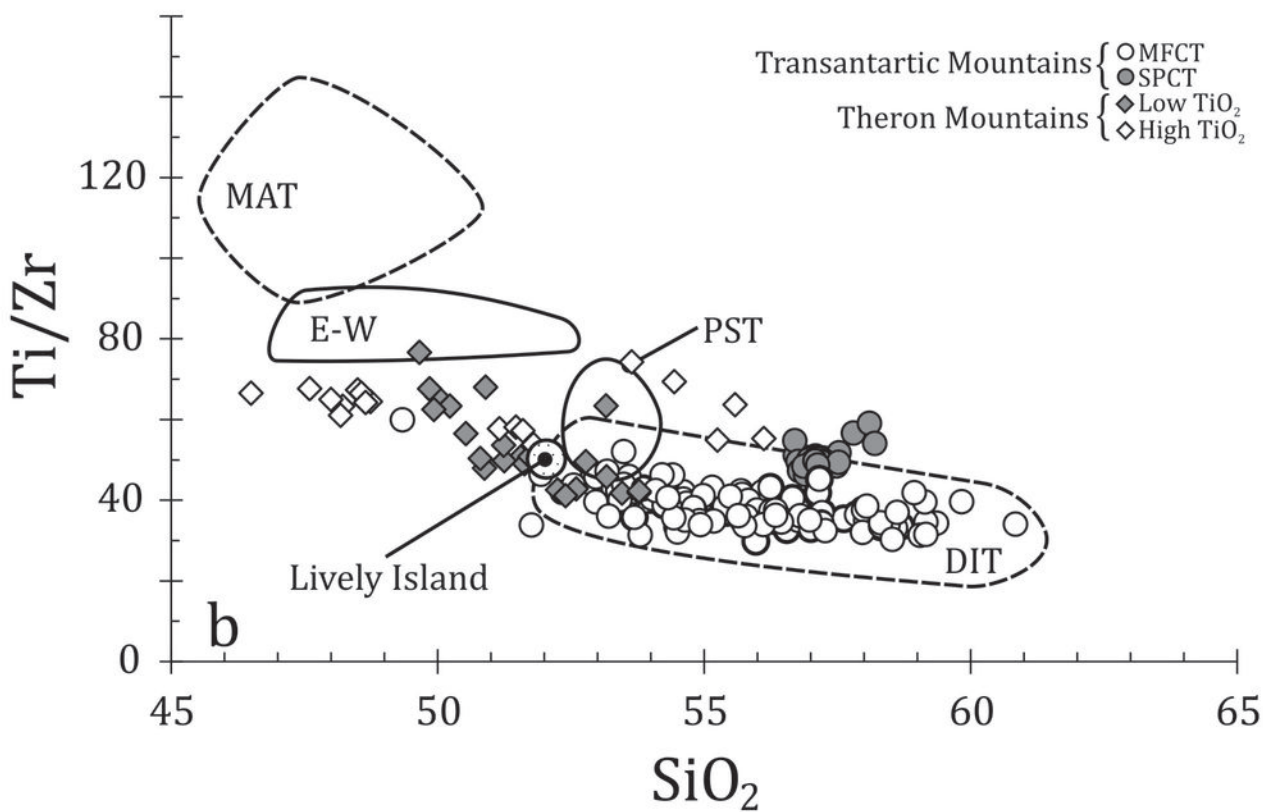
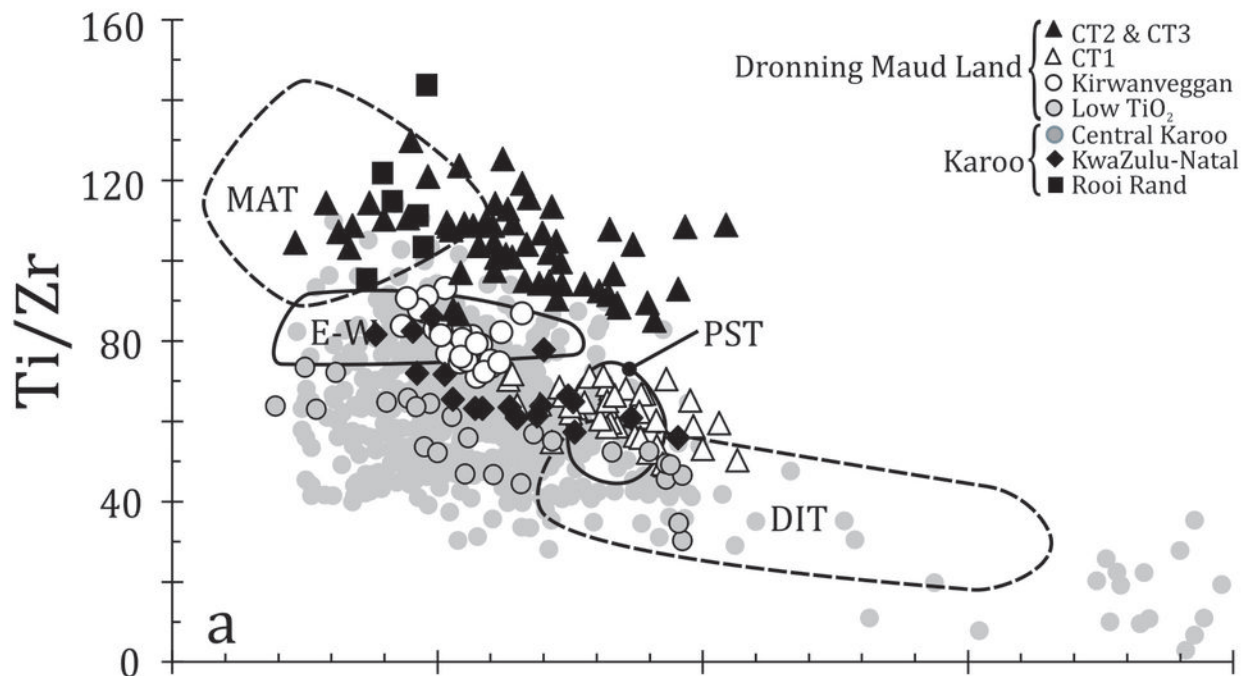


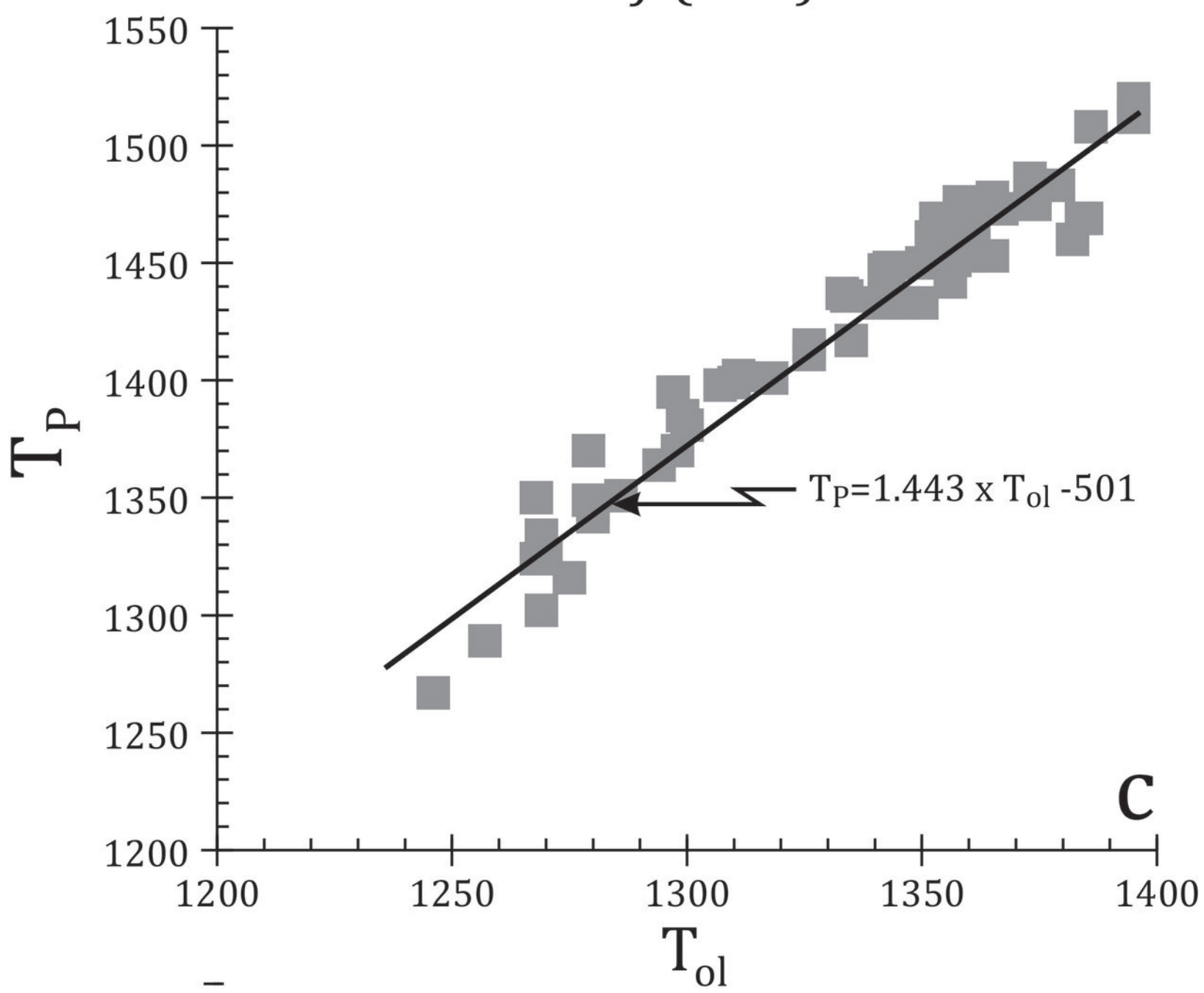
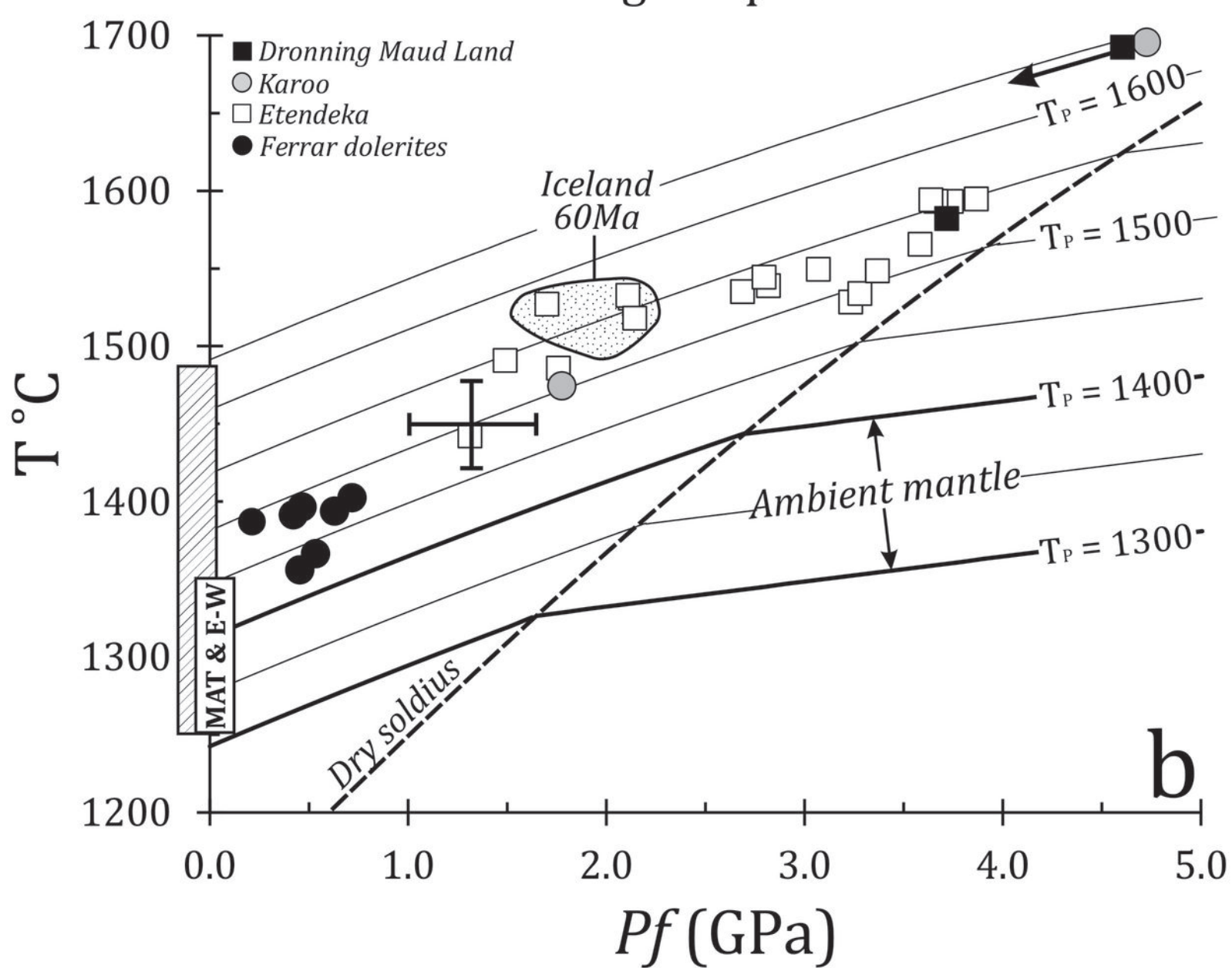
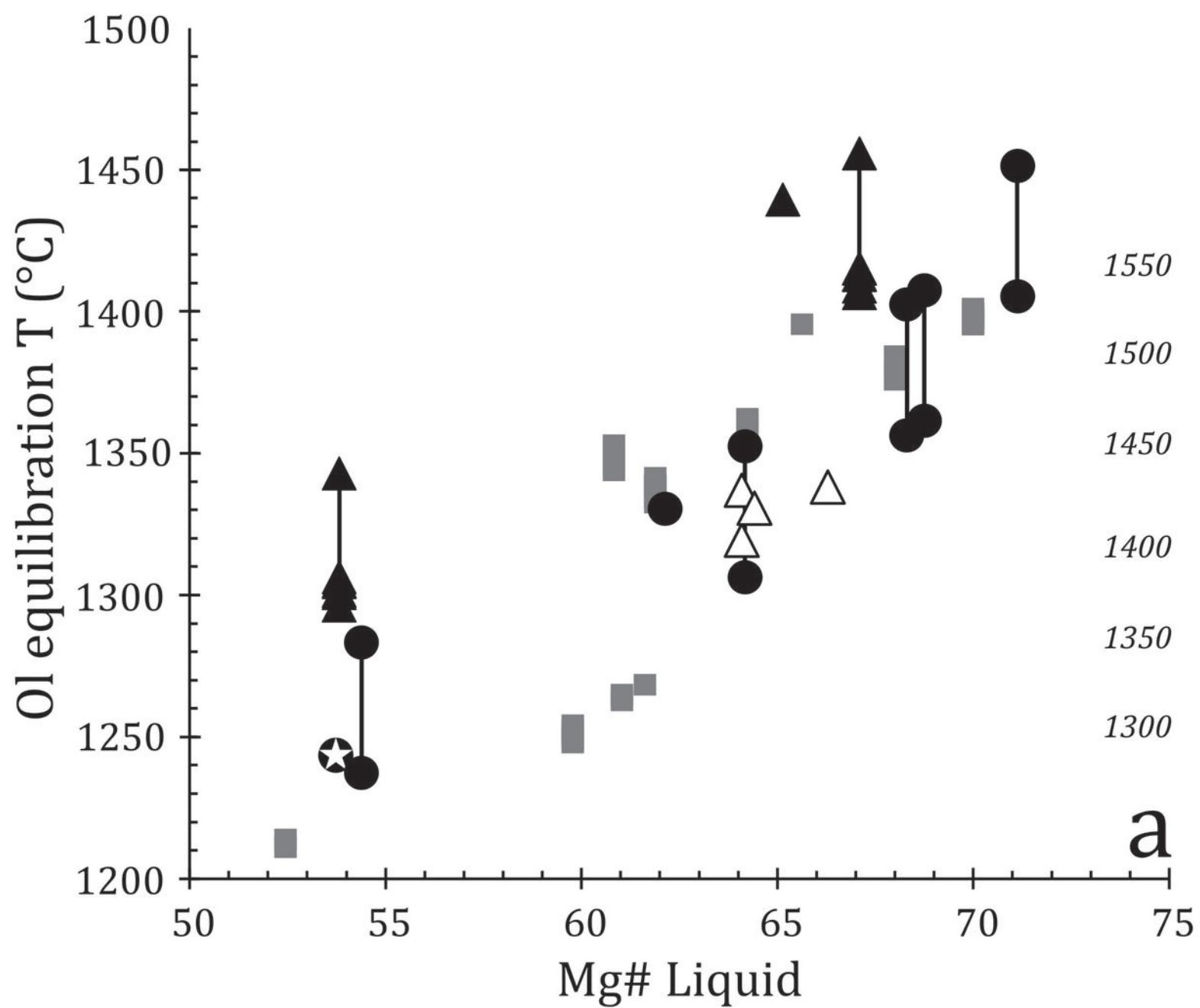












Sample	1187-1	#1503	NEF9	NMF41	MHF1.1	MHF5.5	ECF13	ECF42	ECF44	MHF14.6
Type	PST	PST	PST	PST	PST	PST	EW	EW	EW	EW
SiO <sub>2</sub>	52.67	53.20	52.41	53.59	53.49	53.01	49.49	49.82	50.40	47.02
TiO <sub>2</sub>	0.97	1.02	0.89	1.02	0.99	1.07	1.15	1.21	1.32	0.92
Al <sub>2</sub> O <sub>3</sub>	14.00	12.90	15.69	14.87	13.15	13.90	14.30	14.47	15.22	14.79
Fe <sub>2</sub> O <sub>3</sub>	11.94	11.90	11.50	11.25	11.29	12.03	11.91	11.99	11.85	12.54
MnO	0.14	0.14	0.13	0.17	0.13	0.16	0.17	0.18	0.02	0.19
MgO	7.74	9.43	5.96	6.29	9.15	6.93	9.85	9.14	7.38	10.77
CaO	8.63	8.79	9.35	9.24	8.94	9.18	10.20	10.20	10.87	10.49
K <sub>2</sub> O	2.45	1.90	2.61	2.52	2.10	2.52	2.47	2.58	2.57	2.33
P <sub>2</sub> O <sub>5</sub>	0.98	0.46	0.77	0.92	0.40	0.55	0.36	0.31	0.26	0.41
Na <sub>2</sub> O	0.18	0.16	0.16	0.14	0.11	0.13	0.11	0.11	0.11	0.11
TOTAL	99.70	99.90			99.75	99.48				99.57
Loss	1.50	0.50			1.26	2.62				2.20
Rb	33.1	14.2	22	28	17	22	9	9	8	6
Sr	533	205	256	307	232	234	269	282	283	208
Nb	5.8	4.9	6	6	4.3	4.4	6	5	6	6.9
Zr	110	93	97	106	104	113	80	85	91	81
Y	23.9	23.1	25	23	22	25.1	17	19	24	22.1
Cr	352	625	589	223	577	255	707	449	310	458
Ni	100	170	133	75	146	91	236	174	113	254
Ba	nd	nd	1235	365	250	316	167	144	126	208
La	11.6	9.3	9.35	12.42	10.10	12.90	5.54	5.60	6.55	6.9
Ce	25.1	20.1	20.87	27.19	19.90	24.90	14.19	14.29	16.48	13.5
Pr			2.77	3.44			2.09	2.10	2.45	
Nd	14.7	12.3	12.37	14.64	12.00	15.3	10.01	10.16	11.95	8.6
Sm	3.58	3.15	3.29	3.68	3.34	4.06	2.80	2.84	3.37	2.87
Eu	1.22	1.05	1.12	1.19	1.09	1.28	1.03	1.03	1.20	1.01
Gd			3.76	4.16			3.25	3.29	4.10	
Tb	0.72	0.63	0.64	0.68	0.77	0.79	0.54	0.54	0.68	0.67
Dy			3.98	4.20			3.35	3.35	4.42	
Ho			0.80	0.83			0.66	0.67	0.85	
Er			2.30	2.37			1.87	1.90	2.41	
Tm			0.35	0.36			0.28	0.28	0.36	
Yb	2.14	1.93	2.08	2.12	2.09	2.33	1.66	1.68	2.11	2.34
Lu	0.33	0.28	0.31	0.31	0.32	0.36	0.25	0.25	0.31	0.36
Th	1.83	1.35	1.24	2.14	1.48	2.15	0.67	0.60	0.69	1.0
U	0.80	0.50	0.29	0.51	0.5	0.8	0.37	0.24	0.27	0.7
Ta	0.24	0.19	0.21	0.29	0.18	0.25	0.30	0.23	0.25	0.42
Hf	2.73	2.33	2.6	2.86	2.49	3.03	2.05	2.27	2.48	2.01
Pb			5.55	4.93			2.19	2.65	2.65	
Cs	0.42	0.29			2.24	0.74				0.3
Co	43.30	47.30			50.8	42.9				61.4
Sc	25.70	26.60			27.8	28.2				35
<sup>87</sup> Sr/ <sup>86</sup> Sr	0.71448	0.70900			0.70900	0.70948				0.70600
± 2SE	±1	± 2			± 18	± 17				±2
<sup>87</sup> Sr/ <sup>86</sup> Sr <sub>182</sub>	0.71343	0.70848	0.71083		0.70845	0.70877	0.70579	0.70376	0.70355	0.70578
<sup>143</sup> Nd/ <sup>144</sup> Nd	0.512252	0.512255			0.512259	0.512181				0.512726
± 2SE	±7	±5			± 6	± 6				±7
<sup>143</sup> Nd/ <sup>144</sup> Nd <sub>182</sub>	0.512069	0.512063	0.512367		0.51205	0.511981	0.512561	0.512551	0.512565	0.512475
εNd <sub>182</sub>	-6.4	-6.5	-5.7		-6.7	-8.1	2.9	2.7	3.0	1.6
<sup>206</sup> Pb/ <sup>204</sup> Pb		17.826±11	17.86		18.394 ±8	18.057± 7		18.21		18.474±7
<sup>207</sup> Pb/ <sup>204</sup> Pb		15.622 ±8	15.61		15.658± 8	15.643 ±8		15.47		15.561±8
<sup>208</sup> Pb/ <sup>204</sup> Pb		38.044±19	37.97		38.143±20	38.246±16		37.58		38.111±15
Sample	1187-1	#1503	NEF9	NMF41	MHF1.1	MHF5.5	ECF13	ECF42	ECF44	MHF14.6

Sample	MHF25.1	FAR338	WI-5	MHF18.3	NHF17	MHF14.9	MHF44.1	WI-3	MHF18.1	MHF41.3
Type	Lively	DIT	DIT	DIT	DIT	DIT	DIT Acid	DIT Acid	DIT Acid	DIT Acid
SiO <sub>2</sub>	51.76	52.41	52.44	53.24	53.97	56.06	55.49	60.88	64.11	68.92
TiO <sub>2</sub>	0.82	0.89	1.10	1.30	1.32	1.81	1.54	1.63	1.51	0.71
Al <sub>2</sub> O <sub>3</sub>	15.94	15.69	19.53	15.01	13.27	14.30	15.28	15.24	15.96	15.03
Fe <sub>2</sub> O <sub>3</sub>	10.33	11.5	8.66	12.05	13.88	12.28	12.31	9.19	10.61	6.57
MnO	0.13	0.13	0.12	0.12	0.22	0.18	0.22	0.12	0.06	0.10
MgO	6.38	5.96	6.54	4.99	4.77	2.93	3.48	1.96	1.67	0.60
CaO	11.27	9.35	7.73	8.56	8.68	5.22	5.63	3.01	0.75	0.40
K <sub>2</sub> O	2.46	2.61	2.92	3.21	2.52	4.10	3.76	5.74	3.25	3.51
P <sub>2</sub> O <sub>5</sub>	0.73	0.77	0.22	0.66	1.18	2.06	1.78	1.10	0.75	3.29
Na <sub>2</sub> O	0.17	0.16	0.11	0.17	0.19	0.25	0.20	0.59	0.69	0.21
TOTAL	99.63	99.49	99.36	99.30		99.20	99.69	99.45	99.36	99.34
Loss	1.88	2.10	3.28	3.64		4.12	1.56	2.81	3.30	3.44
Rb	10.9	21.7	29	17.6	34	40.8	40	18.2	20.5	59.6
Sr	231	493.3	582	367	178	358	324	302	1204	715
Nb	10.3	9.1	9.5	12.0	16	18.2	27.4	35.2	74.4	72
Zr	93	96	115	158	192	267	226	309	502	620
Y	21.4	20.0	21.8	30.0	39	41.1	36.2	48.2	85.5	64.8
Cr	172	43	44	71	21	31	11	15	13	19
Ni	63	-	7	95	10	20	6	2.0	8	2.0
Ba	205	494	153	199	371	1409	528	207	2939	862
La	10.8	11.7	16.0	15.7	21.36	26.7	27.0	42.8	47.5	68.9
Ce	21.3	24.1	33.9	32.6	48.50	58.3	55.6	91.9	108	140.0
Pr					6.14					
Nd	11.9	14.7	19.2	20.5	25.93	36.4	29.7	47.0	58.9	69.3
Sm	2.9	3.39	4.41	5.32	6.12	7.92	6.18	10.4	13.2	13.60
Eu	0.92	1.14	1.34	1.63	1.72	2.25	1.77	2.55	3.09	3.41
Gd					6.46					
Tb	0.61	0.60	0.73	0.94	1.07	1.27	1.04	1.55	2.07	2.06
Dy					6.62					
Ho					1.34					
Er					3.91					
Tm					0.62					
Yb	2.41	1.82	2.43	2.81	3.74	3.97	3.62	5.11	7.07	7.47
Lu	0.4	0.28	0.37	0.44	0.056	0.60	0.55	0.76	1.05	1.11
Th	1.68	1.03	1.50	1.49	3.19	2.48	3.90	5.17	5.6	6.54
U	0.8		0.90	0.9	0.77	1.20	1.30	1.70	2.2	2.10
Ta	0.53	0.45	0.62	0.57	0.95	1.04	1.54	2.19	4.32	4.47
Hf	2.32	2.24	3.18	3.78	5.29	5.94	5.53	8.35	11.7	13.80
Pb					13.83					
Cs	0.47		0.28	0.4		0.56	0.38	0.20	0.3	0.20
Co	39.3	21.5	23.20	50.6		35.00	29.4	16.70	12.5	7.40
Sc	37.4	17.1	18.80	15.8		24.70	23.7	18.40	16.3	13.30
<sup>87</sup> Sr/ <sup>86</sup> Sr	0.70564	0.70771±1	0.71042	0.70618		0.70730	0.70730	0.71029	0.71720	0.71745
± 2SE	±15	1	±6	±17		± 17	± 17	± 23	±17	±14
<sup>87</sup> Sr/ <sup>86</sup> Sr <sub>182</sub>	0.70510	0.70733	0.71004	0.70581	0.70594	0.70554	0.70637	0.70983	0.71716	0.71714
<sup>143</sup> Nd/ <sup>144</sup> Nd	0.512505	0.512540±	0.512533 ±8	0.512572		0.512561	0.512561	0.512535	0.512595	0.512542
± 2SE	±8	9		±5		± 6	± 6	± 7	±7	±7
<sup>143</sup> Nd/ <sup>144</sup> Nd <sub>182</sub>	0.512322	0.512374	0.51236	0.512377	0.512259	0.512349	0.512405	0.512369	0.512427	0.512398
εNd <sub>182</sub>	-1.5	-0.6	-0.7	-0.4	-2.8	-0.9	3.1	-0.6	0.6	-0.1
<sup>206</sup> Pb/ <sup>204</sup> Pb	18.781±9	17.980±9	18.067±9	18.430±8				18.016±10	18.326±8	18.393±6
<sup>207</sup> Pb/ <sup>204</sup> Pb	15.670±9	15.510±8	15.512±8	15.633±7				15.508±10	15.576±8	15.529±6
<sup>208</sup> Pb/ <sup>204</sup> Pb	38.300±23	37.361±18	37.425±12	37.944±2				37.492±26	37.880±20	37.583±12

Sample	MHF15.2	MHF14.4	MHF15.1	MA1
Type	MAT	MAT	MAT	MAT
SiO <sub>2</sub>	45.92	47.40	48.56	47.51
TiO <sub>2</sub>	1.81	1.52	1.71	1.39
Al <sub>2</sub> O <sub>3</sub>	15.70	16.39	16.71	16.45
Fe <sub>2</sub> O <sub>3</sub>	13.60	13.23	12.52	12.91
MnO	0.16	0.17	0.21	0.20
MgO	8.00	7.51	7.15	8.27
CaO	10.59	10.65	9.80	10.05
K <sub>2</sub> O	2.59	2.53	2.53	2.65
P <sub>2</sub> O <sub>5</sub>	0.30	0.05	0.17	0.38
Na <sub>2</sub> O	0.20	0.17	0.19	0.20
TOTAL	98.87	99.63	99.56	
Loss	1.5	1.90	2.25	
Rb	4.7	5.5	2.0	10
Sr	424	444	381	396
Nb	11.2	9.9	10.7	7
Zr	80	79	80	90
Y	21.1	18.6	18.2	19
Cr	89	78	95	89
Ni	119	102	121	116
Ba	110	105	103	827
La	8.1	8.0	7.9	4.37
Ce	18.0	17.2	18.3	11.45
Pr				1.83
Nd	13.3	12.8	13.8	9.73
Sm	3.72	3.32	3.78	3.08
Eu	1.38	1.25	1.42	1.29
Gd				3.72
Tb	0.7	0.63	0.72	0.61
Dy				3.66
Ho				0.71
Er				1.97
Tm				0.30
Yb	2.05	1.83	2.04	1.69
Lu	0.32	0.28	0.33	0.23
Th	0.42	0.42	0.48	0.26
U				0.09
Ta	0.58	0.54	0.6	0.3
Hf	2.28	1.94	2.26	2.60
Pb				1.07
Cs	0.3	0.35	0.2	
Co	48.2	42.60	49.3	
Sc	28.9	25.40	28.6	
<sup>87</sup> Sr/ <sup>86</sup> Sr	0.70400	0.70385±17	0.70342	
± 2SE		±14	±15	
<sup>87</sup> Sr/ <sup>86</sup> Sr <sub>182</sub>	0.70392	0.70375	0.70338	0.70497
<sup>143</sup> Nd/ <sup>144</sup> Nd	0.512747	0.512743	0.512738	
± 2SE	±6	±17	±6	
<sup>143</sup> Nd/ <sup>144</sup> Nd <sub>182</sub>	0.512537	0.512548	0.512532	0.512588
εNd <sub>182</sub>	2.8	3.0	2.7	3.6
<sup>206</sup> Pb/ <sup>204</sup> Pb	19.152±6	17.858±7	18.131±7	17.91
<sup>207</sup> Pb/ <sup>204</sup> Pb	15.656±5	15.476±6	15.579±7	15.50
<sup>208</sup> Pb/ <sup>204</sup> Pb	38.464±13	37.425±18	37.762±16	37.57

Table 1. Whole-rock major and trace element and isotopic compositions of Falkland Islands intrusions used in this study. Major elements and isotopic compositions for sample numbers starting with EC, NE, NH, NM and MA are from Mitchell *et al.* (1999) with addition trace elements from this study. See supplementary materials for analytical methods.

Table 2. Geochemical, mineralogical and petrographical characteristics of the different groups of Falkland Islands intrusions.

Type	Type locality	Mitchell <sup>1</sup>	Stone <sup>2</sup>	Petrographic features	Mineralogy	Subgroup	Mg#	SiO <sub>2</sub>	TiO <sub>2</sub>	Ti/Zr	Zr/Y	<sup>87</sup> Sr/ <sup>86</sup> Sr <sub>182</sub>	εNd <sub>182</sub>
Port Sussex Creek (PST)	Port Sussex 51°40'15" S 58°58'41" W	N-S	NE-SW	Coarse-grained dolerite	Pig ± Opx + Aug Rare Ol + Di	none	48-58	52-54	0.9-1.2	50-70	3.6-5.3	0.7077 -0.7134	-5.5 to -10.9
E-W	Fox Bay West 51°57'02" S 60°05'21" W	E-W	E-W	Coarse-grained olivine dolerite	Ol + Plag ± Aug	none	42-64	47-54	1.0-1.9	77-90	3.2-4.8	0.7036-0.7058	-0.4 to +3.0
Lively Island (LI)	Lively Island 52°00'00" S 58°27'47" W	Lively Island	NE-SW	Coarse-grained with accessory biotite	Ol + Plag + Aug ± rare pigeonite	none	48-52	51-52	0.8-0.9	53	4.0-4.54	0.7053	-0.5 to -1.4
Dyke Island (DIT)	Dyke Island 51°59'33" S 60°52'50" W	Not defined	Radial swarm	Fine-grained aphyric, rarely plagioclase ± augite-phyric	Plag + Aug	Acid	<22	62-75	0.2-1.6	<31	5.0-8.8	0.7055-0.7098	-2.8 to -0.5
						Low TiO <sub>2</sub>	27-57	52-61	1.1-1.7	24-67	4.8-7.4		
						High TiO <sub>2</sub>	41-51	53-58	>1.80	25-53	6.8-8.4		
Mount Alice (MAT)	Mount Alice 52°09'12" S 60°35'55" W	Mount Alice	Radial swarm	Fine-grained plagioclase ± olivine phyric	Ol + Plag ± Aug	none	44-64	47-50	1.3-1.9	98-142	3.2-5.2	0.7031-0.7039	0.0 to +3.7

1. Groups described by Mitchell *et al.* (1999); 2. Groups defined by Stone *et al.* (2009)



Calculated extract for fractionation of PST and E-W intrusions

	<b>PST</b>			<b>E-W</b>		
	NGF16	MHF5.1	Calc	ECF12	ECF44	Calc
SiO <sub>2</sub>	54.01	53.81	53.82	49.69	51.03	50.98
TiO <sub>2</sub>	0.94	1.00	1.13	1.05	1.21	1.36
Al <sub>2</sub> O <sub>3</sub>	13.20	14.97	15.02	13.30	15.21	15.20
FeO	10.60	10.62	10.60	10.51	11.11	11.06
MnO	0.20	0.17	0.18	0.17	0.17	0.21
MgO	9.67	6.78	6.78	11.62	6.71	6.70
CaO	8.81	9.50	9.49	9.81	11.51	11.50
Na <sub>2</sub> O	1.96	2.62	2.56	2.29	2.56	2.46
K <sub>2</sub> O	0.48	0.42	0.56	0.32	0.39	0.39
P <sub>2</sub> O <sub>5</sub>	0.12	0.11	0.15	0.11	0.11	0.13
Extract			%			%
Olivine	Fo <sub>83</sub>		0.0			57.0
Plagioclase	An <sub>70</sub>		18.9			40.4
Pyroxene	En <sub>71</sub> Fs <sub>19</sub> Wo <sub>9</sub>		74.7			
Pyroxene	En <sub>51</sub> Fs <sub>13</sub> Wo <sub>33</sub>		6.4			2.6
Σ residuals <sup>2</sup>			0.127			0.038
F			0.79			0.75

Table 4 AFC parameters for the trajectories shown in Fig. 12. R is the ratio of assimilated rock to crystal cumulate. A value appropriate for upper-crustal contamination has been used. F is the total amount of crystallization required to reach the most extreme composition on a particular trajectory.  $T_{\text{CHUR}}$  is the Chondritic Uniform Reservoir model Nd age for the most extreme composition on a particular trajectory, in Ga.

		AFC parameters								$T_{\text{CHUR}}$ (Ga)
		Sr	Nd	$\epsilon\text{Nd}$	$^{87}\text{Sr}/^{86}\text{Sr}$	$D_{\text{Sr}}$	$D_{\text{Nd}}$	R	F	
<b>CT1</b>	Source	50	5	2	0.7035	0.5	0.1	0.40	$\leq 0.2$	3.0
	Crust	400	20	-50	0.7120					
<b>PST-1</b>	Source	60	4	2	0.7035	0.5	0.1	0.40	$\leq 0.2$	2.2
	Crust	350	40	-20	0.7200					
<b>PST-2</b>	Source	100	5	2	0.7035	0.5	0.1	0.40	$\leq 0.2$	1.8
	Crust	350	60	-10	0.7250					